Journal of *Marine Science and Engineering*

MDPI

Article

A Modular and Scalable Approach to Hybrid Battery and Converter Integration for Full-Electric Waterborne Transport

Ramon Lopez-Erauskin [1,*], Argiñe Alacano [1], Aitor Lizeaga [1], Giuseppe Guidi [2], Olve Mo [2], Amaia Lopez-de-Heredia [3] and Mikel Alzuri [3]

[1] Faculty of Engineering, Mondragon Unibertsitatea, Loramendi 4, 20500 Arrasate-Mondragón, Spain; aalacano@mondragon.edu (A.A.); alizeaga@mondragon.edu (A.L.)
[2] SINTEF Energy AS, Sem Sælands vei 11, 7034 Trondheim, Norway; giuseppe.guidi@sintef.no (G.G.); olve.mo@sintef.no (O.M.)
[3] IKERLAN, José María Arizmendiarrieta Pasealekua 2, 20500 Arrasate-Mondragón, Spain; alopezheredia@ikerlan.es (A.L.-d.-H.); malzuri@ikerlan.es (M.A.)
* Correspondence: rlopez@mondragon.edu

Abstract: This paper presents a flexible and scalable battery system for maritime transportation, integrating modular converters and hybrid battery technologies that are effectively implemented in real-world scenarios. The proposed system is realized with modular DC-DC converters, which do not require complex design and control or a high number of components and combine high-power (HP) and high-energy (HE) battery cells to optimize the energy and power requirements of vessel operations without oversizing the energy storage system. Moreover, the modular design ensures flexibility and scalability, allowing for easy adaptation to varying operational demands. In particular, the system topology, control mechanisms, and communication protocols are explained in this paper. The concept has been validated through simulations and real-scale laboratory tests, demonstrating its effectiveness. Key results highlight the system's ability to maintain the DC bus voltage while operating at high efficiency (ranging from 97% to 98%) under different load conditions, supported by reliable and demanding real-time communication using the EtherCAT standard. This real-time capability has been validated, and related results are presented in this paper, showing a synchronization accuracy below 200 ns between two modules and a stable control at a cycle time of 400 µs. This approach offers a promising solution for reducing greenhouse gas emissions in the maritime industry, aligning with global sustainability goals.

Keywords: DC-DC power converter; electric vessel; energy storage system (ESS); EtherCAT; hybrid; modular converter; real time

check for updates

Academic Editor: Qiuwan Shen and He Miao

Received: 28 November 2024
Revised: 27 December 2024
Accepted: 6 January 2025
Published: 11 January 2025

Citation: Lopez-Erauskin, R.; Alacano, A.; Lizeaga, A.; Guidi, G.; Mo, O.; Lopez-de-Heredia, A.; Alzuri, M. A Modular and Scalable Approach to Hybrid Battery and Converter Integration for Full-Electric Waterborne Transport. *J. Mar. Sci. Eng.* **2025**, *13*, 120. https://doi.org/10.3390/jmse13010120

Copyright: © 2025 by the authors. Licensee MDPI, Basel, Switzerland. This article is an open access article distributed under the terms and conditions of the Creative Commons Attribution (CC BY) license (https://creativecommons.org/licenses/by/4.0/).

1. Introduction

In 2023, waterborne transport accounted for approximately 3–4% of CO_2 emissions in the European Union, which corresponds to about 15% of the emissions from the transportation sector [1]. European ships alone produced 128.2 million tons of CO_2 emissions, roughly 18% of the global CO_2 emissions from maritime transport [2]. Indeed, maritime transport could face a 50–250% greenhouse gas (GHG) emission increase by 2050 if carbon-intensive modes of transport continue to grow as expected [3]. In 2023, the International Maritime Organization (IMO) formulated a revised strategy aligned with the Paris Agreement objectives to achieve net-zero GHG emissions from the shipping industry by 2050, relative to the emissions recorded in 2008 [2].

Therefore, waterborne transportation, including ships, ferries, and other vessels, is increasingly transitioning toward electrification. This shift aims to reduce emissions, improve efficiency, and enhance sustainability. As a result, electric propulsion systems play a key role in achieving these goals.

In terms of energy consumption and efficiency, electric propulsion systems must handle different types of loads. For example, during high peak demands (such as acceleration or maneuvering), vessels require significant power output, and electric propulsion systems must cope with these peaks efficiently. However, at cruising speed, power demands are more stable. Hence, optimizing energy usage during this phase is essential for overall efficiency.

The use of hybrid energy sources has been a common solution in the electrification of waterborne transportation. In this kind of solution, hybrid vessels combine batteries with other energy sources (e.g., fuel cells, diesel generators, or solar panels) [4]. In order to combine different energy sources efficiently, energy storage systems (ESSs) help in "shaving" peak power demands by providing additional energy during acceleration or other high-load scenarios. This prevents overloading the main fuel-based power source (e.g., diesel generators) and ensures smoother operation. ESSs also allow vessels to operate in zero-emission mode when relying solely on batteries.

In this scenario, either as support or as the main source of power, batteries are a common choice for energy storage in waterborne transportation [5–7]. Among various options, lithium-ion batteries (LIBs) are particularly effective in cutting down pollutant emissions by reducing the reliance on diesel generators during port stops, which significantly lowers fuel consumption [8]. In fact, when comparing different battery technologies (lithium-ion, nickel–hydrogen, lead–acid), LIBs stand out as the leading choice for ship electrification due to their high energy density, long lifespan, quick response times, relatively low maintenance, and the safety standards required for ships [9,10]. Indeed, LIBs are highlighted as the most widely used electrochemical storage systems due to their high power and specific energy. These characteristics make them suitable for scalability and adaptability in large transportation systems, particularly in marine applications [11].

Considering the current state of the electric waterborne transportation described here, it is worth remarking that in the scope of this research, hybridization refers to combining different battery technologies in full electric vessels with no fuel-based energy sources. A hybrid topology that combines high-energy (HE) battery cells and high-power (HP) battery cells reduces the size of the ESS while providing sufficient energy and power to meet the ship's demands. Additionally, this hybrid topology removes the high-current stress factor from the HE battery, resulting in a longer lifetime and smaller temperature peaks in the cells and eliminating the effect of a high depth of discharge.

Typically, energy storage systems onboard maritime vessels rely on a single type of battery cell technology. Consequently, a monotype battery, usually of the HE type, is employed for various energy-demand scenarios (such as maintaining cruising speed, maneuvering, or fast charging), without distinguishing between HE and HP operations. HP battery cells typically offer greater cycling capacity compared to HE cells [12,13]. This characteristic is crucial for applications requiring rapid power delivery, such as maneuvering, peak-shaving, and other fast transient power demands. As a result, the monotype HE battery system often has surplus energy with low cycling capacity, leading to increased costs, weight, and volume and reduced flexibility. Hybrid energy storage systems (HESSs) combining different battery technologies offer the advantage of adapting their use depending on whether HE or HP demand is required. This optimizes the storage system, eliminating the need for oversized batteries. Therefore, accurately determining the optimal size of the HESS is essential to take advantage of the benefits of hybridization.

In recent years, many combinations of electrical energy storage have been studied to suit ship applications in terms of price, autonomy, and lifetime [14,15]. However, to date, hybrid energy storage systems have not been generally used in waterborne transport.

Therefore, the system proposed in this paper focuses on a battery system combining different converters and cell technologies, all integrated in a modular way. In fact, the development of solutions that integrate ESS (based on batteries) together with power electronic converters is interesting in different applications, such as, for example, electric vehicles (EVs), where the integration of ESS and power electronic converter improves the overall performance regarding EVs internal structure development, motor speed and torque regulation, voltage compensation, voltage boost, and power flow control [16].

In addition, integrating hybrid energy storage technologies together with power electronic converters in a modular solution allows flexibility in capacity adjustments and makes the systems scalable, ensuring that vessels can adapt to changing operational requirements. As technology evolves, vessels can upgrade or expand their energy storage capacity without major overhauls. In addition, a modular system has the following advantages: (i) independent power flow control on each module to extend the lifetime of the ESS (and e.g., equalize, degradation per module), (ii) higher reliability, as a defective module can in principle be bypassed, keeping the battery string in operation until such module is replaced, and (iii) cost saving, as module characteristics do not need to be matched strictly to ensure optimal system performance, lowering the cost of production considerably and enabling different generations of batteries to be used in the same string, which is a great advantage given the quick development of cell technology.

The recent literature highlights significant advancements in integrating power electronic converters with high-energy and high-power batteries for electric vessels. Gajardo et al. proposed a modular multilevel matrix converter (M3C) that utilizes hybrid energy storage systems, combining fuel cells and batteries to enhance propulsion and grid supply capabilities in marine vessels [17]. Long et al. introduced a modular multilevel converter with integrated composite energy storage, effectively addressing power fluctuations and providing emergency supply during grid faults [18]. However, multilevel converters require complex control and design and face limitations such as voltage unbalance or reliability. In addition, as they require a large number of components, their cost is higher.

Anzola et al. explored partial power processing converters, demonstrating their modularity and efficiency, achieving a peak efficiency of 99.36% in a 3 kW prototype, which is crucial for battery charging in maritime applications [19]. However, partial power processing converters have not yet been implemented in a modular way, and their cost may not be as competitive as other topologies. In addition, these architectures still have to cope with some limitations such as complexity, galvanic isolation, additional protection circuits, and managing large voltage differences.

Additionally, Yinhe et al. described an integrated power system for battery-only electric ships, emphasizing the combination of supercapacitors and lithium batteries for enhanced power management [20].

In particular, several papers discuss the implementation of battery-based storage systems and the integration of power electronic converters in all-electric vessels. Ayers highlighted the role of lithium-ion batteries in enabling zero-emission operations for high-speed electric vessels, emphasizing the importance of DC rapid charging systems to accommodate shorter docking times [21]. Trombetta et al. reviewed the integration of large-scale battery energy storage systems (BESSs) in the shipping industry, detailing the regulatory framework and technical considerations necessary for their deployment [11]. He et al. analyzed over 750 commercial BESS installations, providing insights into decision-making, cost-effectiveness, and operational performance, while also addressing the need

for improved converter efficiency during low-power operations [22]. Lastly, Chen and Wang proposed a design for containerized battery energy storage systems, which includes charge and discharge control mechanisms suitable for electric vessels [23].

Collectively, these studies underscore the potential of advanced power electronics in optimizing energy storage and management in electric maritime systems [16], but they do not provide effectively implemented solutions in real-world scenarios [16]. Therefore, this work emphasizes the application of hybrid and modular solutions, which combine different battery cell technologies and integrate them with relatively simple power electronic converters that do not require a large number of components or complex control systems, and a variety of experimental work and system performance evaluation is provided [12,13]. Modularity, however, brings the need for coordinated control and accurate synchronization between DC-DC converters embedded in the modules. In fact, the modular control of the system implies cycle time, latency, and jitter below 500 µs, 100 µs, and 1 µs, respectively, in order to provide sufficient synchronization accuracy between the control signals in the DC-DC converters of different modules. A deterministic, low-latency communication protocol is necessary to achieve these real-time requirements. Such requirements are common in industrial factory automation, and there are several communication standards that adjust to these applications. In waterborne electric transportation, however, to the best of our knowledge, such stringent timeliness and synchronization requirements are not common, and the communication protocols used in these applications do not match the aforementioned real-time requirements. In this research, communication standards commonly used in factory automation applications have been considered as a solution to fulfill the real-time requirements for the modular control of the system. Several industrial protocols (EtherCAT, Ethernet/IP, PROFINET, Ethernet Powerlink, and SERCOS III) have been analyzed, given their capability to achieve sub-microsecond synchronization accuracy [24–26]. Eventually, EtherCAT was selected due to its overall real-time performance, low protocol overhead, widespread availability, and ease of implementation.

Finally, another aspect to take into account when designing and implementing any energy supply system, and even more so in maritime applications, is reliability. In particular, redundancy and fail-safe mechanisms are critical to prevent disruptions during operation. The presented modular converters concept makes the system inherently redundant.

In summary, electrification, efficient propulsion, battery-based storage, and reliability considerations are driving the adoption of energy storage systems in waterborne transportation. Hybrid solutions and scalable designs offer promising solutions for a sustainable maritime industry. Therefore, this paper presents an HESS focusing on two main improvements that are independent of each other: hybrid battery cells and modular converters. A modular converter is not strictly necessary for a hybrid battery, but it is one way to interface with hybrid storage systems. In addition, the modular power converter would also be beneficial for monotype energy storage systems, i.e., systems based on a single battery cell technology. The paper is divided into the following sections: Section 2 describes the HESS system. Sections 3 and 4 are devoted to the control and communication proposed in this paper, respectively. Then, Section 5 presents simulation results, Section 6 validates the proposed approach, and, finally, Section 7 draws some conclusions.

2. System Description

The HESS system considered in this research would be connected directly to a DC connection point on a vessel's DC bus or power system. The target vessels or potential use cases of a HESS could be electrical urban ferries or harbor tugs. Urban ferries have a relatively high number of cycles as their nominal operation but with additional energy requirements for the batteries under certain circumstances. These applications have the

most predictable operational profiles. Tugs are vessels specially designed to assist the other ships during maneuvers by forcing or tugging them toward the port and transporting the floating artifacts from one place to another [27]. These types of vessels usually have a primary cycle (the most common cycle that a vessel performs), which is relatively small compared to their overall energy requirement and is performed at a relevant, high number of times per day.

In this context, the HESS would be responsible for supplying the energy and power required to meet the vessel's energy demand. This demand would, therefore, be met by a series of batteries and adapted by various power electronic converters. Figure 1 shows the overall scheme of the whole system.

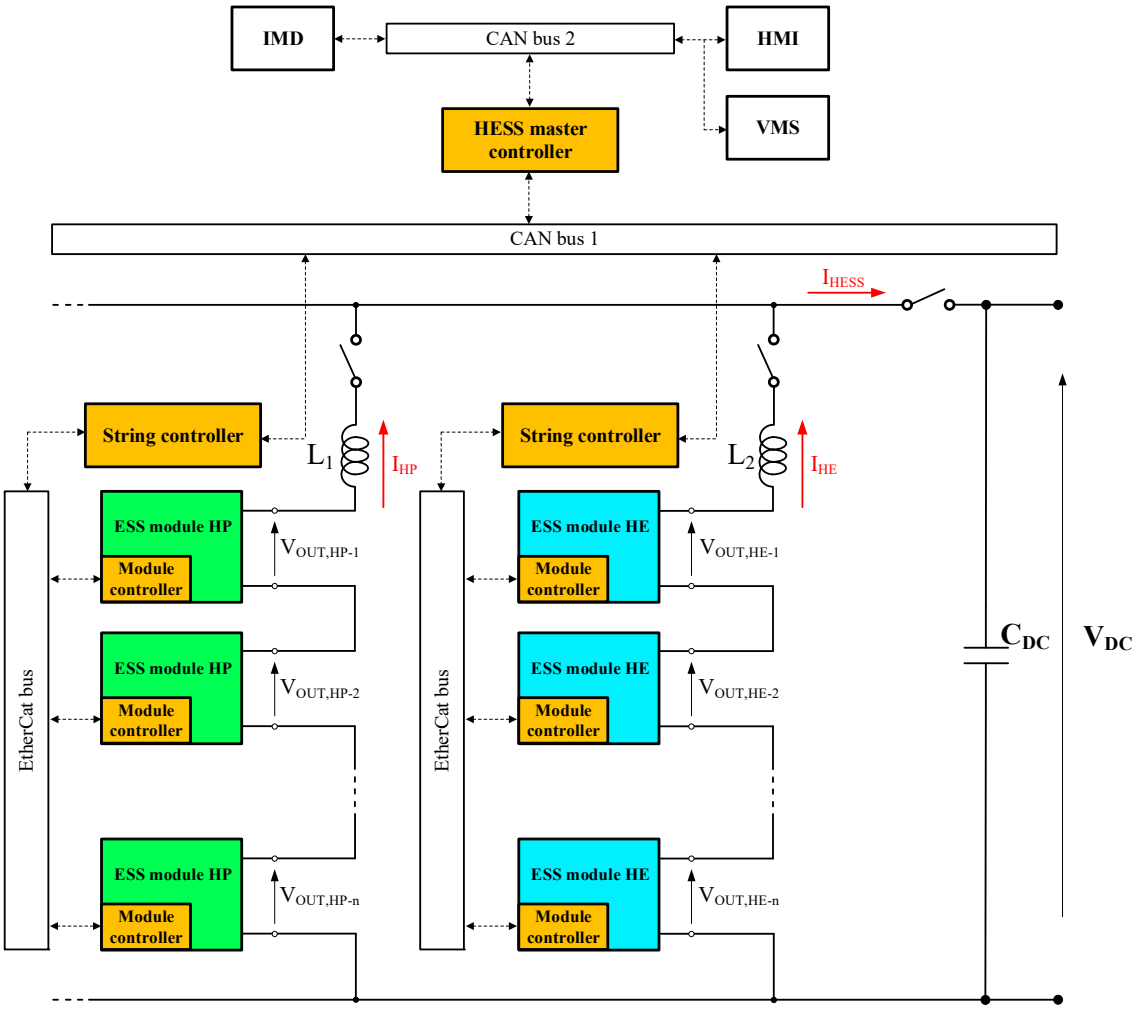

Figure 1. HESS system configuration comprising HP and HE modules, communication networks, and the controllers.

Usually, the ship's electrical system is relatively complex, with AC and DC buses and different power sources. Furthermore, some of the components can be redundant and used to improve reliability, while others are used to improve power management and operability.

In this context, the proposed HESS is designed to operate as the main power source or even as an additional source in the case of further battery or fuel cell systems regulating the DC bus voltage on all-electric vessels. However, by managing the connection of the modules, the system can generate a regulated voltage in both DC and AC and can, therefore, be connected directly to the on-board power system without a need for additional power converters, thus being able to adapt to different bus types (DC or AC).

The core concept behind the system under consideration involves modularizing the power converter, which, in this case, is a DC-DC converter. Each battery module comprises multiple battery cells and a bidirectional DC-DC converter, forming an energy storage system module (ESS module), described in Section 2.1. These ESS modules are interconnected in series to form a string. Then, by connecting strings in parallel, the desired DC voltage, power rating, and energy storage capacity are achieved. The proposed design, as illustrated in Figure 1, facilitates the integration of both HE and HP battery cells within the same system. While HE and HP cells must be placed into separate strings to fully exploit this combination, strings with different cell types can operate in parallel. However, the proposed topology, i.e., a series connection of ESS modules, makes it possible to use or combine ESS modules with different characteristics (voltage, capacity, etc.) or cell technology within the same string as well.

In this topology, the different battery system controllers can manage the power sharing between HE and HP cells. This is possible because the power flow in each module can be controlled, and HE and HP cells are placed in separate strings. It is important to note that the proposed HESS system does not require a precharge system to power up as long as the sum of module voltages exceeds the DC bus voltage. In this scenario, the precharge system becomes redundant, as current control allows for connection without any current flow.

Several control modes have been implemented to make the hybrid system flexible for integration into vessel DC power systems utilizing different power management strategies. As mentioned before, the battery system can be configured to control the vessel DC bus voltage, and a droop control can be activated in case other battery systems or other sources of power, such as fuel cells, are also configured to control the same bus voltage. The system can alternatively be operated in current or power control mode if the battery system is intended to feed into a DC grid whose voltage is controlled by other sources. This mode can also be used to control the charge power.

The power management strategies for the vessel itself, like strategies for power sharing between batteries and other onboard power sources, are outside the scope of this paper. This also applies to strategies for optimal utilization of a hybrid battery system. The presented system, with its implemented control, is able to control the power sharing according to what is desired. However, the optimal way of splitting power between the strings with different cell types is not within the scope of this paper. Strategies for optimal sharing can either be implemented directly in the HESS master controller, or the HESS master controller can take commands from a higher-level power management system.

2.1. ESS Module

As mentioned before, a battery module and a DC-DC converter form the ESS module (Figure 2). Typically, the voltage of individual ESS modules falls within the range of 50–120 V. The battery module includes battery cells connected in series and parallel and battery management systems (BMSs) for local balancing and cell monitoring of voltages and temperatures. HE cells are lithium nickel manganese cobalt oxide (NMC) type, and HP cells are lithium titanate oxide (LTO) type, which are common cell technologies in electric ships [11,19,27,28]. LTO and NMC batteries are prominent choices for marine applications due to their characteristics that make them suitable for the marine environment. LTO batteries are known for their high safety, long lifespan, and ability to operate over a wide temperature range, making them ideal for withstanding extreme conditions at sea. On the other hand, NMC batteries offer high energy density and excellent fast-charging capabilities, which are crucial for applications requiring a large amount of energy in a limited space. Additionally, NMC batteries have a prolonged lifespan and are lighter, contributing to the

efficiency and maneuverability of vessels. These combined features make both technologies highly valued in the marine industry, providing reliable and efficient energy solutions.

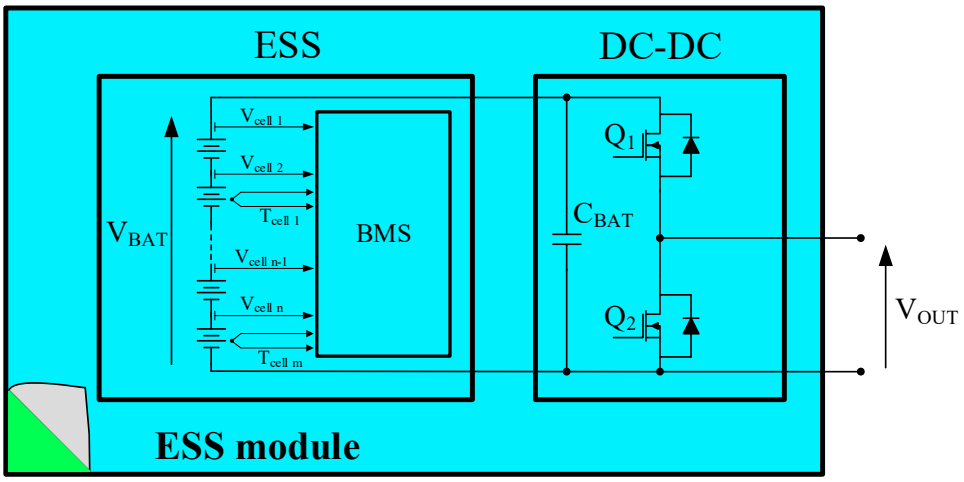

Figure 2. ESS module details, including battery cell distribution, BMS, and DC-DC converter topology.

HE and HP module characteristics considered for the HESS system are gathered in Table 1. Cell-level characteristics of the NMC and LTO batteries are detailed in [27].

Table 1. HE and HP battery module characteristics.

Cell Type	Manufacturer/ Model	Configuration	C-Rate	Voltage (min.–nom.–max)	String Capacity (Configuration)	Maximum Current
HE NMC	Samsung SDI 94 Ah	1p28s	1	78.8 V–102.2 V –120.4 V	190 kWh (12 × 15.84 kWh)	155 A
HP LTO	Toshiba SCiB 23 Ah	2p44s	4	66.0 V–101.2 V –118.8 V	56 kWh (12 × 4.66 kWh)	184 A

In each module, a standard pulse-width modulation (PWM) half-bridge converter serves as the bidirectional and DC-DC converter. Thus, the DC-DC cannot step up the battery voltage. To build a cost-oriented solution, the same DC-DC converter is designed for both HE and HP modules. The rating values of this converter (based on Table 1) are as follows: nominal voltage of 100 V, voltage operation range between 80 V and 120 V, and maximum current of 184 A. The equation that relates the battery and output voltages of the ESS module represented in Figure 2 at steady-state operating conditions is given by the general expression of the buck converter operating at steady-state conditions:

$$V_{\mathrm{OUT}} = D \cdot V_{\mathrm{BAT}} \tag{1}$$

where V_{OUT} and V_{BAT} are the output and battery voltages of the ESS module, respectively, and D is the duty cycle value ranging from [0–1]. V_{BAT} depends on the number of series-connected cells (N_{S}) within each module:

$$V_{\mathrm{BAT}} = \sum_{i=1}^{N_{\mathrm{S}}} V_{\mathrm{cell}i} \tag{2}$$

and the voltage of the i-th cell ($V_{\mathrm{cell}i}$) depends on its current state of charge (SoC).

The current and voltage characteristics of both HE and HP modules are similar (see Table 1), so it has been decided to use the same converter design for both HE and HP modules, reducing the complexity and the cost of the design. Thus, the designed DC-DC

converter must be able to operate at 120 V and supply 184 A. The characteristics of the main components of the converter are the following: the switching frequency is $f_{SW} = 5$ kHz, the input capacity $C_{BAT} = 48$ µF, and the maximum drain-source voltage of the switching MOSFETs $V_{DS} = 200$ V. In addition, the main characteristics of the inductor in each string are $L = 163$ H, $I_{DC} = 184$ A, and $\Delta I = 20\%$.

2.2. Strings

The full system consists of one or more strings, with each string comprising several series-connected ESS modules, as illustrated in Figure 1. Within each string, a shared inductor is connected in series with all the ESS modules. The purpose of the inductor is to limit the current and to allow string current control, as it is the main element that allows energy storage.

The output voltage requirements of the system determine the minimum number of ESS modules in each string. The sum of voltages across all series-connected cells within the string ($N_{S,string}$) at the lowest SoC must exceed the minimum required output voltage of the battery system that, in this case, is equal to the minimum DC bus voltage ($V_{DC.min}$) allowing operation of the power system of the vessel. The following assumes that all cells have the same characteristics:

$$N_{S,string} \cdot V_{cell,min} > V_{DC,min} \tag{3}$$

where $V_{cell,min}$ is the cell voltage that corresponds to the lowest value of $SoC = SoC_{min}$. Under this assumption, (2) can also be expressed as follows:

$$V_{BAT.min} = N_S \cdot V_{cell,min} \tag{4}$$

and (3) can be expressed as follows:

$$N_{S,mod} \cdot V_{BAT,min} > V_{DC,min} \tag{5}$$

If the inequality in (5) is not fulfilled, the duty cycles of all converters will be operating at $D = 1$ according to (1), and the step-down operation could not be performed.

2.3. Full HESS

The full battery system consists of several parallel connected strings, some of which contain HE modules, while others contain HP modules (see Figure 1). Each individual string is designed to ensure the minimum required voltage ($V_{DC,min}$) for the entire battery system. The HESS system's DC power (P_{HESS}) is given by the product of the DC bus voltage (V_{DC}) and the current flowing from the HESS into the system (I_{HESS}):

$$P_{HESS} = V_{DC} \cdot I_{HESS} \tag{6}$$

with I_{HESS} being the sum of all HE and HP string currents connected in parallel to the DC bus:

$$P_{HESS} = V_{DC} \cdot \left(\sum_{i=1}^{N_{P,HE}} I_{HEi} + \sum_{i=1}^{N_{P,HP}} I_{HPi} \right) \tag{7}$$

where $N_{P,HE}$ and $N_{P,HP}$ are the number of HE and HP strings, respectively, connected in parallel and contributing to the current flow of the system.

3. System Control

As mentioned above, the HESS is in charge of supplying the necessary energy and power to the vessel, which normally varies over time. Therefore, the HESS needs a control system that takes into account the limits of the batteries and converters and adapts to the variability of energy consumption while maintaining a stable DC bus voltage.

The proposed control is organized into different levels in a hierarchical structure. At the lowest level is the ESS module control, which is responsible for operating the DC-DC converter according to the instructions received from the string controller and acts as a BMS master. At the intermediate level is the string control, which is in charge of monitoring the modules and giving orders such as enable/disable or duty cycle to the low-level control (module) according to the orders received from the high-level control (HESS master). The string controller is also responsible for the balancing process between all modules in the string. Finally, at the highest level is the HESS master control, which is in charge of controlling the output voltage or power flow depending on the vessel requirements and, in addition, determining the power split between HE and HP. Next, these control levels are described in more detail.

3.1. ESS Module Control

The module control has two different functionalities. On the one hand, it is in charge of controlling the DC-DC converter depending on the information it receives from the string controller. The module control receives the duty cycle reference sent by the string controller and outputs the PWM signal of the DC-DC converter gate drivers. This way, the output voltage of the module is established, which will take values between zero (total bypass of the module) and the total voltage of the battery cells connected in series.

On the other hand, the module controller implements master BMS functions and reports the module battery status to the string controller. The local BMS units monitor cell voltages and temperatures to ensure the system stays within safe operating conditions. Measurements are transmitted to the module controller that (i) calculates the SoC, state of health (SoH), and state of function (SoF) at cell and module levels, (ii) applies the cell balancing algorithm, and (iii) reports faulty cells or any anomaly to string control.

3.2. String Control

Individual string controllers manage the power flow within each string. The strings receive current or voltage references from the HESS master controller via CAN bus, represented in blue solid line boxes in Figure 3. Internally generated references are represented in red dashed line boxes. The HESS can program the string to operate in either the current control mode or voltage control mode. In the former case, the HESS gives directly the reference value for the current to be supplied (or absorbed) by the string. In the latter case, the HESS gives a reference for the bus voltage, and the reference for the inner current control loop is generated by the string controller itself via an external control loop (voltage control loop), as shown in Figure 3. In any case, the output of the inner current control loop provides the total voltage to be generated by the series connection of all modules.

As can be seen in Figure 3, in case the string is in voltage control mode, a droop compensation is active, ensuring that the string can be operated in parallel with other strings operating in voltage control mode. Moreover, the droop compensation ensures load sharing between parallel units. The K_{droop} gain can be set individually, which allows the strings to contribute to a different degree of the total required power.

Besides voltage/current control, the string controller is also responsible for optimizing the power split between modules within the string by setting the appropriate duty cycle for each individual module. The algorithm used for duty cycle calculation applies PWM

modulation to only one module in each string at a time and lets the other modules output zero or full voltage to reduce overall switching losses. The string control decides which module should output zero, full, or regulated voltage (PWM) and when to change the operating mode of each module based on the information received from each module, i.e., SoC, SoH, SoF, etc., via the EtherCAT link (orange solid line box in the figure).

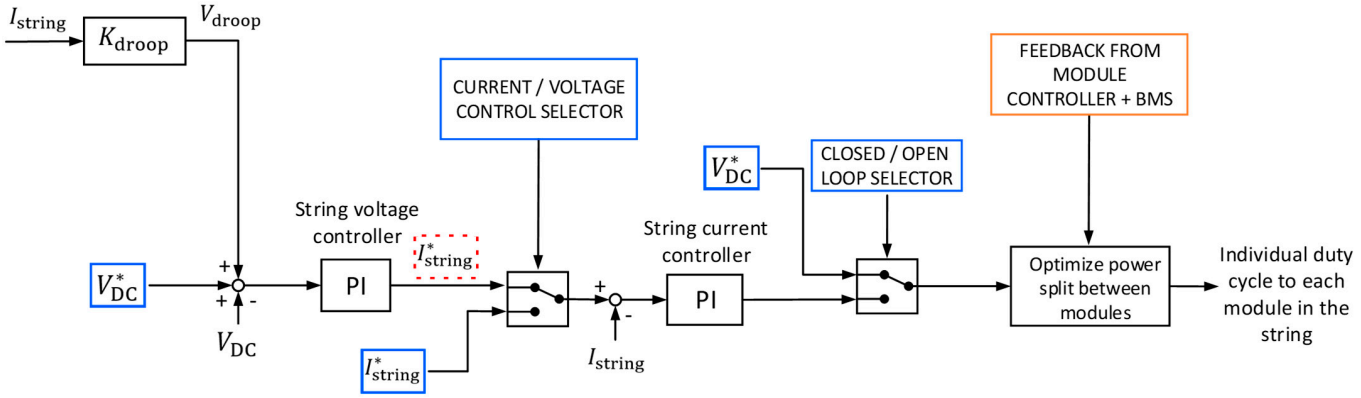

Figure 3. String control diagram and functionalities.

3.3. HESS Master Control

A HESS master controller controls either the DC bus voltage of the system or the total power flow in and out of the battery. The selection of the control mode depends on the desired performance of the system connected to the battery. Typically, the required control mode and reference values for voltage or current are commanded from the vessel management system (VMS) or the local human–machine interface (HMI), although internal reference values are also available. Furthermore, the HESS master control may determine the power split between HE and HP strings. This can be determined by various rule-based algorithms, although, in this case, it has been done by means of a low-pass filter (LPF) applied to the HE current reference. In this way, the response of the HE string is slower, causing the HP string to handle the fast transients. Figure 4 shows the HESS master control diagram, in which external commands from HMI/VMS via CAN bus are represented in blue solid line boxes, and internally generated references in red dashed line boxes. The output references and commands sent to the strings will depend on the control mode selected from the HMI/VMS.

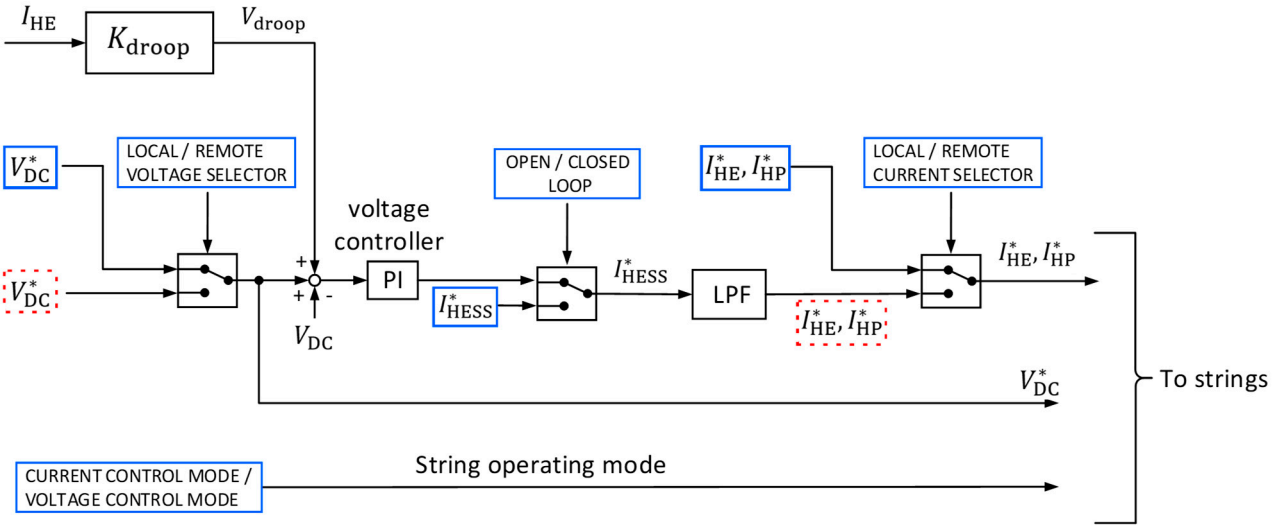

Figure 4. HESS master control diagram.

The main functionalities of the HESS master control are described below:

- Direct current control: the HESS system is only responsible for controlling the output current, with each string following its designated current reference. Under this condition, the DC bus voltage needs to be controlled by a power source external to the HESS system.
- Controlled DC bus voltage: the output voltage of the full system is controlled and can be maintained at a constant level in case the HESS system is the only power source controlling the DC bus voltage. Instead, if more power sources connected in parallel to the DC bus implement output voltage control, droop-based control is activated. Implementing droop-based output voltage control enables efficient power sharing between the battery system and other power sources. The key advantage of droop control is that power sharing will not depend on a central controller and the communication between the systems [29,30].
- Controlled battery power flow: in some specific applications, e.g., when charging from an external DC source, managing the power flow of the battery system may be preferable over controlling the output voltage. This power control functionality can be implemented in the master controller, allowing the battery system to receive power commands from the VMS or the local HMI.

Apart from the aforementioned functions, the HESS master control is responsible for monitoring the isolation of the system by means of an insulation monitoring device (IMD) and provides the required information to the HMI or VMS: available HESS power and energy, monitoring of the strings and modules, logging of cell, module and string information, load requirements, etc.

As pointed out in Section 2, the proposed system has potential use cases in urban ferries and/or harbor tugs. Therefore, the control modes described above have been implemented.

For example, the droop control mode is beneficial in case more sources connected in parallel are also operating in voltage control mode. This situation can happen in case the vessel power supply is supported by other power sources apart from the HESS, for example, in a full-electric vessel with other battery systems or fuel cells or even in a not fully electric vessel with diesel engines. Droop mode is adequate for cruising speed operation (navigation), as well as for maneuvering operations like docking. Indeed, the profile used in Sections 5 and 6 for validating the different control modes mimics navigation at a constant speed (constant power/current demand), maneuvering (power demand variation, i.e., increase/decrease of power demand), and battery charging (negative current).

However, the HESS can be the only system in charge of controlling the DC bus voltage, which is why the HESS voltage control mode has been implemented.

Finally, the power or current control mode is particularly useful in certain scenarios, such as charging from an external DC source (when the ship is docked, for example), where it might be more advantageous to regulate the battery system's power flow rather than its output voltage.

4. HESS System Communication

The distributed control and characteristics of the system described in the previous sections require all the involved devices to communicate between them. PWM synchronization between modules and high bandwidth closed loop current control impose stringent real-time requirements for the communication infrastructure. The whole communication scheme of the presented system, divided into three topological hierarchy levels, is addressed in this section.

The diagram in Figure 1 not only represents the system layout and element hierarchy discussed in previous sections but also the three communication levels in which the system is organized:

String level communications between the string controller and the module controllers. PWM synchronization issues and high bandwidth closed loop control are addressed at this communication level.

HESS level communications between the HESS master controller and the string controllers. System level control is addressed at this communication level.

HMI level communications between the HMI and the HESS master controller. User level monitoring and commanding are addressed at this communication level.

In the following subsections, each communication level is described in detail.

4.1. String Level—Communications Between the String Controller and the Module Controllers

At this communication level, each string controller commands the battery modules connected to it to control the DC bus voltage or string current according to the commands and references set by the HESS master controller. As aforementioned, the PWM signals in the DC-DC converters of each module within a string must be synchronized in order to establish the string current and the DC bus voltage properly and avoid instability issues and large ripple currents. As long as modules are synchronized, the maximum (steady state) ripple voltage across the string inductor will be limited to the maximum module voltage. To fulfill these requirements, the communication links between the string controllers and their corresponding module controllers are based on the EtherCAT standard protocol. EtherCAT has been chosen after a comparative analysis of some potentially suitable industrial communication protocols. This comparative analysis is summed up in Table 2.

Table 2. Industrial Ethernet protocols' real-time characteristics comparison [24–26,31].

Feature	EtherCAT	SERCOS III	Ethernet/IP	Ethernet Powerlink	PROFINET
Cycle time [µs]	~10	~30	~1000	~200	<100
Jitter [µs]	<1	<1	~1	<1	<1
Latency [µs]	1–100	~1	~1000	<1000	~1000
Protocol overhead	Low (process "on-the-fly")	Medium (real-time channels)	High (TCP/IP)	Low (TDMA)	Medium (TCP/IP UDP/IP)
Ease of implementation	Moderate (wide support)	Complex (support focused on motion control)	Easy (standard Ethernet tools)	Moderate (specialized stack)	Moderate (wide range of tools and libraries)
Open-source support	High (SOEM, commercial stacks)	Low (few open-source options)	Moderate	Moderate	Moderate
Hardware cost	Medium (standard Ethernet MAC, specialized ASICs)	High (specialized hardware)	Low (standard Ethernet MAC)	Low (standard Ethernet MAC)	Low (standard Ethernet MAC)

In terms of real-time features, both EtherCAT and SERCOS III stand among the rest of the options. SERCOS III, optimized for motion control, outperforms EtherCAT in terms of latency. However, EtherCAT's low protocol overhead, ease of implementation enabled by open-source software stacks, and hardware cost-effectiveness position it as the preferred standard for communication between string controllers and module controllers. In conclusion, EtherCAT's real-time characteristics—featuring cycle times and latency below 100 µs, communication jitter below 1 µs, and low data overhead—combined with hardware cost-effectiveness and software support availability, make it a suitable choice for the application addressed in this research. Experimental results demonstrating communications' compliance with these real-time requirements are detailed in Section 6.3.

Regarding the communication topology at this communication level, each string comprises an EtherCAT network and is composed of one string controller and several

module controllers. The string controller plays the master role, and module controllers play the slave role in the EtherCAT communication network. The network topology is shown in Figure 5, with only one master node and a number of slave nodes connected to it. For simplicity, a single daisy-chain connection from the master to all slaves is implemented. The possibility of implementing a ring topology to improve the reliability and availability of the system, which is part of the original EtherCAT standard specifications, is left to further development.

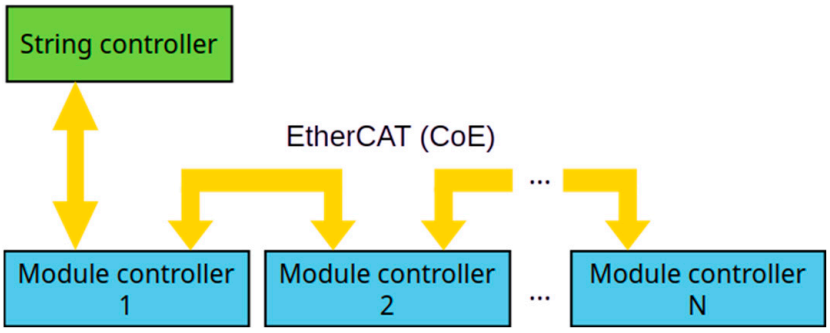

Figure 5. Network topology between the string controller and the module controllers.

Concerning data transfer between string and module controllers, string controllers send synchronization frames, operation commands, and process control references to their respective module controllers every 400 µs, which is the control cycle time in the strings. Additionally, they also receive various information from their module controllers, such as module alarms, status, cell voltages, cell temperatures, etc., at the same rate. Using this information, the string controllers perform control operations over their modules, send control data back to the HESS master controller and close control loops at the HESS master controller level, and send monitoring data to the HESS master controller to be displayed on the HMI. Further details on data exchange between string and module controllers are given in Appendix B.

In terms of software development, it is worth mentioning that the implementation of the EtherCAT master nodes (string controllers) software is based on the Simple Open EtherCAT Master (SOEM) v1.4.0 [17], while the implementation of slave nodes (module controllers) software is based on the EtherCAT Technology Group's EtherCAT Slave Stack Code ET9300 standard [32]. Both implementations include CANopen over EtherCAT (CoE) as the application layer communication protocol.

4.2. HESS Level—Communications Between HESS Master Controller and the String Controllers

All the information to control the entire system's operation is transmitted and received at this communication level. The HESS master controller commands the string controllers' operation by setting the references for DC bus voltage, current, power, or strings' current according to the configuration and parameters set by the user in the HMI. Additionally, string controllers also send various information to the HESS master controller, such as string controller's alarms, status, measured voltage, current, etc. Using this information, the HESS master controller performs control operations at the HESS level and sends monitoring data to the HMI. The layout of this communication level is given in Figure 6.

Unlike in the string communication level, no hard real-time requirements are needed at the HESS level. Voltage, current, and power controls performed at this level are run at a cycle time of 10 ms instead of the sub-millisecond order of the string communication level. The results shown in Sections 5.1 and 6.4 prove that this cycle time is appropriate to carry out HESS level control correctly. Considering these time constraints and the industrial application of this research, the communication link between the HESS master

controller and the string controllers is based on a CAN bus due to its robustness, reliability, cost-effectiveness, and implementation ease.

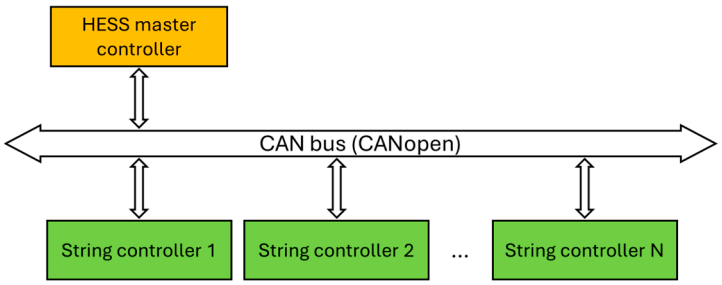

Figure 6. HESS system CAN bus communication scheme.

Regarding data transfer between HESS and string controllers, the HESS controller sends synchronization frames, operation commands, and process control references to the string controllers every 10 ms. As a direct response to the synchronization frames, string controllers send operation state, measurements, and other necessary information for system control back to the HESS controller every 10 ms. Further details on data exchange between the HESS master controller and string controllers are given in Appendix B. Given the complexity and the amount of data transmitted between the HESS master controller and the string controllers, a standardized high-communication layer protocol has been adopted. Specifically, the CANopen protocol has been implemented over the CAN bus communications between the HESS master controller and the string controllers. The implementation of this CANopen communication is based on the open-source CANopenNode project [33].

4.3. HMI Level—Communications Between the HMI and the HESS Master Controller

The primary objective of this communication level is to provide users with the manual control of the system. To achieve this, the HMI is enabled to monitor and command various data and actions within the HESS–strings–modules control process. For example, users can open or close the HESS master's and string controllers' contactors, select the HESS master controller's operation modes, and set reference values for system voltage, current, power, etc. In terms of monitoring, the HMI displays information such as the status of the HESS master and string controllers, voltage, current, and power measurements of the string controllers, voltage and temperature of the modules' cells, etc. To carry out data exchange, as shown in Figure 7, the HMI and the HESS master controller are interconnected via a CAN bus, and they are programmed with a custom-designed minimalistic application layer communication protocol.

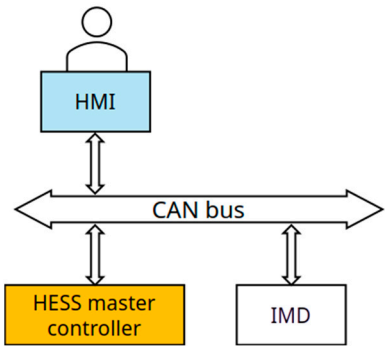

Figure 7. HMI communication level layout.

In addition to the HMI and the HESS master controller, an IMD is also connected to this CAN bus. Its purpose is to monitor the state of the isolation system and communicate it to the HESS master controller. This IMD is the Sensata Sendyne SIM100MOD, which is equipped with a CAN interface and operates with its own application layer communication protocol. It functions as a data producer in polling mode, with the HESS master controller periodically polling the IMD to obtain DC bus insulation status information. If any error or warning is reported by the IMD, the HESS master controller will stop the operation of the whole system and bring it to a safe state until a correct isolation status is reported again by the IMD. It is worth mentioning that the IMD operates at a fixed transmission rate of 500 kbits/s. Consequently, the HMI and the HESS master controller must also operate at the same transmission rate.

Given the characteristics of the application at this communication level, stringent real-time requirements are not necessary. However, it is worth mentioning that a 100 ms cycle time has been defined, which has been considered short enough for monitoring purposes. Every cycle, the HESS master controller sends monitoring data to the HMI and polls insulation state information from the IMD, and the HMI sends a Keep Alive message to the HESS master controller. Further details on data exchange between the HESS master controller, HMI, and IMD are given in Appendix B.

5. Simulation Results

The simulations are carried out in MATLAB-Simulink environment following the system architecture in Figure 1. The HESS system is composed of two strings, one with HP modules and the other with HE modules. Each string is composed of 12 modules connected in series. Modules include average models of the converter and the battery with parameters from Table 1 and [26]. The vessel power system comprises a DC-link capacitor of $C_{DC} = 10$ mF accounting for its equivalent series-resistance $ESR = 100$ mΩ and a variable load that follows the profile in Figure 8. The system follows the hierarchy described in Section 2 and includes the controllers corresponding to each control level explained in Section 3.

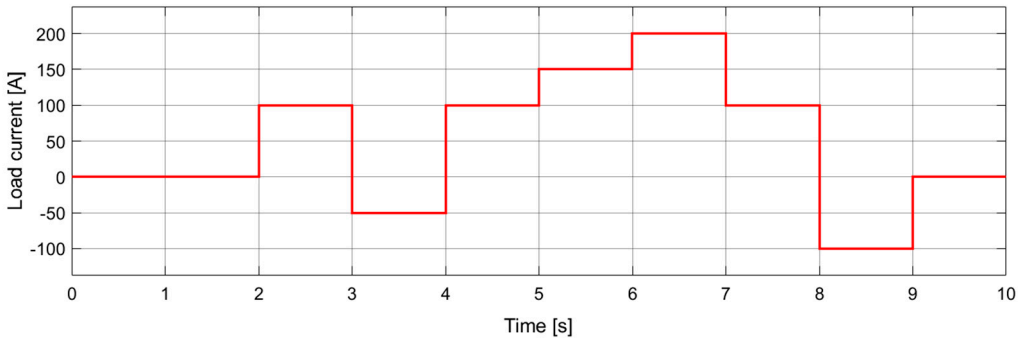

Figure 8. Load current profile applied to the system.

5.1. HESS Master Voltage Control Mode Simulation

Figure 9 illustrates the full system operating under the HESS master voltage control mode. Due to the simulation step size, the duration of the simulation was adequate to show the performance of the control system under perturbations. The control implements a soft-start ramp-up from 0 V to the nominal voltage of 1000 V. The load demand variation is fulfilled by the voltage PI controller ($K_P = 1.6$, $K_I = 20$) in charge of setting the current references to the HP and the HE strings. The latter implements LPF with a time constant of 100 ms to slow down the transient response of HE batteries. HP batteries support the required peak demands during these transitions. Modules with HE batteries are limited to

180 A maximum to avoid overcurrent situations. Under these circumstances, HP batteries also support the load demand (for the time period $t = 6$ s $- 7$ s in Figure 9, bottom plot).

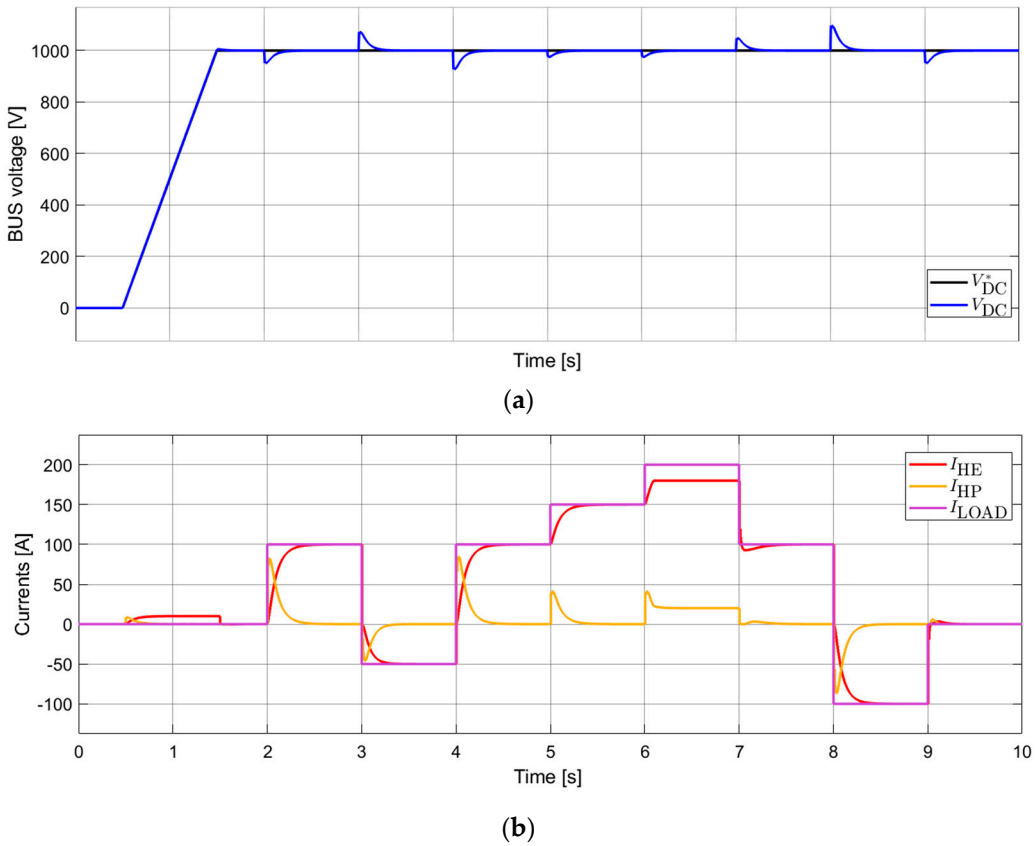

Figure 9. HESS master voltage control simulation: (**a**) DC bus voltage reference and measurement and (**b**) current measurements of the HE and HP strings and the load.

In Figure 9, it can be seen that, in the face of disturbances, the control system is able to maintain the DC bus voltage within acceptable limits in this type of application, specifically between +/−10% of nominal voltage.

5.2. HESS Master Droop Control Mode Simulation

Droop control is also possible at the HESS master control level. As stated before, this control mode is beneficial in case more sources connected in parallel are also operating in voltage control mode. Figure 10 shows the operation of the HESS system and an additional source operating in parallel. Both implement droop control with the same gain of $K_{droop} = 100$ V/180 A. Figure 10 (top) presents the DC bus voltage reference (V^*_{DC}) alongside the actual DC bus voltage (V_{DC}). The variation in V_{DC} is influenced by the load demand and the droop gain implemented in each of the sources. Figure 10 (bottom) illustrates the currents of the HE and HP strings, the additional source, and the load. Given that the droop gain is identical for both the HESS and the additional source, each source shares half of the load demand.

Figure 10 shows that, in the face of disturbances, the control system operating in droop mode is still able to maintain the DC bus voltage within acceptable limits (within +/−10% of the nominal voltage).

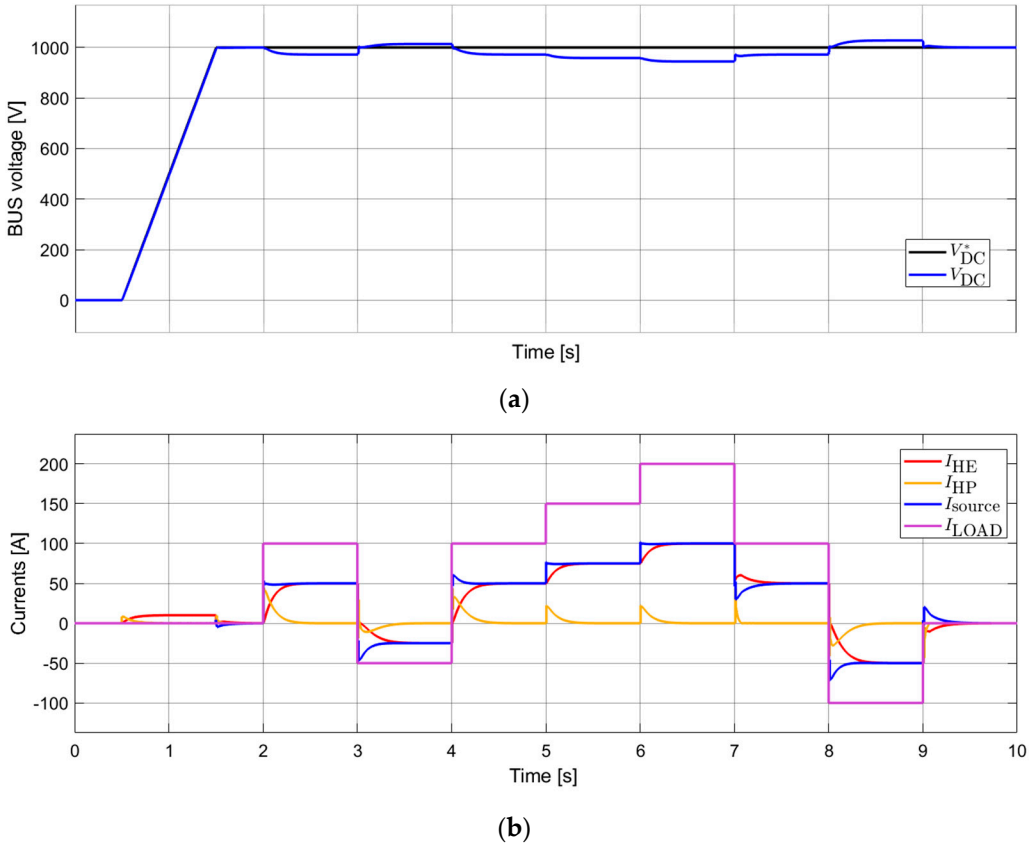

Figure 10. HESS system and another source in parallel in droop mode, both regulating the DC bus voltage: (**a**) DC bus voltage reference and measurement and (**b**) current measurements of the HE and HP strings, parallel source, and load. Due to the simulation step size, the duration of the simulation was adequate to show the performance of the control system under perturbations.

6. Experimental Results

This section is focused on the experimental results of (i) DC-DC converter operation, (ii) module controller synchronization, (iii) SoC optimization of modules, and (iv) full-system operation. Detailed description of the different test platforms dedicated to each type of test is provided, and additional information about the experimental set-ups is given in Appendix A.

6.1. DC-DC Converter Characterization

The objective of this section is to validate the designed DC-DC converter as a component level. Different tests are carried out: switching and conduction tests to analyze the behavior of semiconductors, overcurrent protection test, isolation tests, and buck mode operation tests. Figure 11 shows buck mode operation test set-up diagram. The objective of these tests is the characterization of the DC-DC converter, and to perform tests in buck mode, some additional components are needed. Therefore, the test bench also includes the following: an inductor of $L = 170$ µH connected in series at the positive terminal of the converter's output, which stores energy when the MOSFET is ON and releases it when it is OFF; an output capacitor of $C = 3$ mF to eliminate undesired noise and fluctuations in the output voltage; and a variable load $R_{LOAD} = [0.45\ \Omega - 2.1\ \Omega]$ to operate the converter at the required power level.

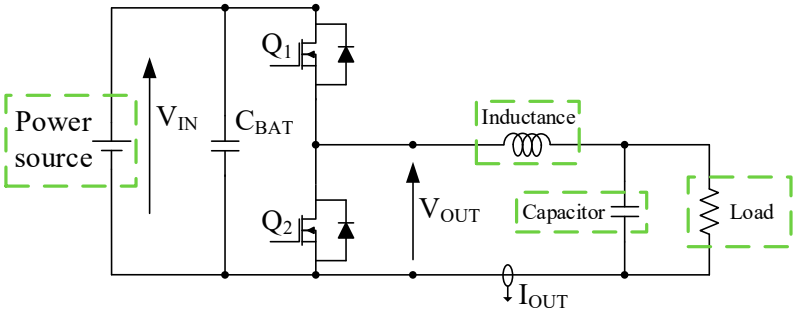

Figure 11. Buck mode operation test set-up diagram. The elements identified with dashed green rectangles are additional components allowing characterization tests to be performed.

Figure 12 shows the DC-DC converter performance at different operating points. Figure 12a shows the output voltage points obtained at different input voltage and duty cycle values. Test results show the converter performance at three input voltage values ($V_{IN} = 90$ V, $V_{IN} = 100$ V, and $V_{IN} = 120$ V) and six duty cycle values ($D = 0.2$, $D = 0.5$, $D = 0.6$, $D = 0.7$, $D = 0.8$, and $D = 0.9$). The input and output V/I ratio appears in Figure 12b, and the output power achieved is shown in Figure 12c. The maximum power point is $P_{OUT} = 18.56$ kW at $V_{OUT} = 100.99$ V and $I_{OUT} = 183.64$ A, showing the ability of the converter to provide the rated power. Figure 12d illustrates the efficiency of the converter, ranging from 97% to 98%. It is worth noting that these tests were carried out below 50 °C ambient temperature.

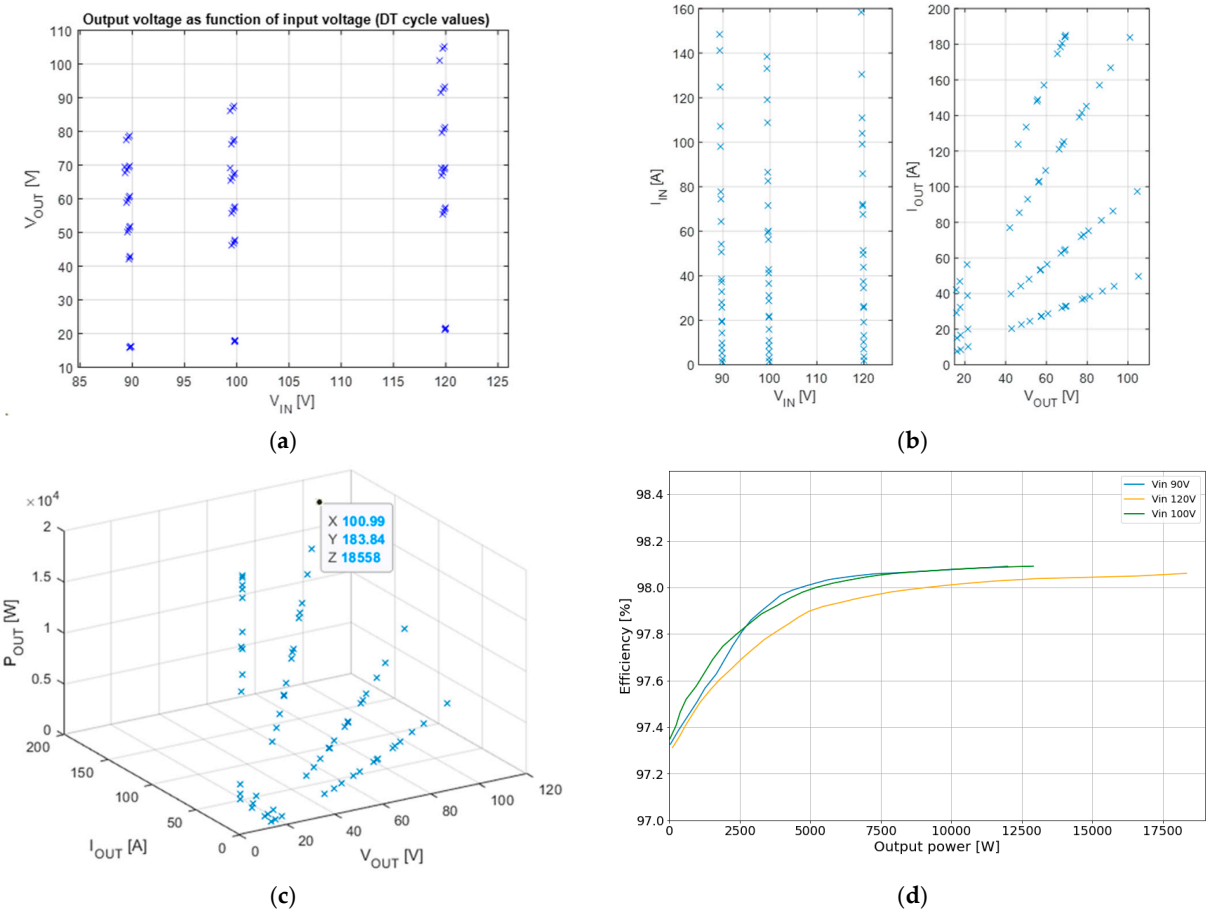

Figure 12. DC-DC converter performance at different operating points: (**a**) V_{OUT} vs.V_{IN} for a set of duty cycle values. (**b**) Input and output current vs. voltage curves operating at variable output load conditions. (**c**) P_{OUT} as function of V_{OUT} and I_{OUT}. (**d**) Efficiency curves at different input voltages.

6.2. Single Module Validation Under Normal Operating Conditions

These tests, as described in the set-up diagram of Figure 13, aim to validate the operation of a single module consisting of a BMS (represented in the light blue box), a DC-DC converter (purple), and a module controller (dark blue) under normal operating conditions. The variable load (red) and the variable power source (dark green) described in Section 6.1 are also required for these tests, as well as a battery cell emulator (light green) directly connected to the BMS input ports that allow emulating under- and over-voltage situations in individual cells.

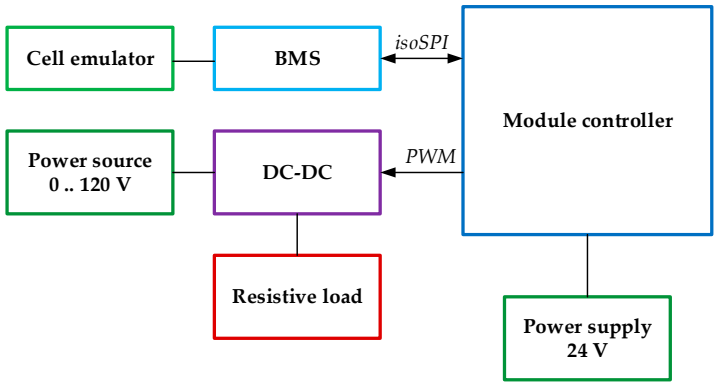

Figure 13. DC-DC converter, BMS, and module controller test set-up diagram.

Table 3 gathers a set of operating points performed on the DC-DC converter. Considering that the converter is operating in buck mode, V_{DC} corresponds to the input voltage of the converter, V_{LOAD} is the output voltage, and I_{LOAD} is the output current. Figure 14 shows the waveforms and average values of one of the tested operating points, where $V_{DC} = 120$ V (green) is the bus voltage imposed by the power supply (Figure 11), $V_{LOAD} = 51.6$ V (yellow) is the voltage at the load terminals, $I_{LOAD} = 147$ A (purple) is the current through the load, and $V_{OUT} = 52.1$ V (blue) is the voltage at the output of the converter switches considering a $R_{LOAD} = 0.35\ \Omega$. It is worth noting that no noise or switching-related effects were observed at any of the tested operating points. Changing the duty cycle value and the DC source value, different V_{LOAD} and, thus, different I_{LOAD} can be tested to assure that the DC-DC converter performances are adequate in all the operation ranges.

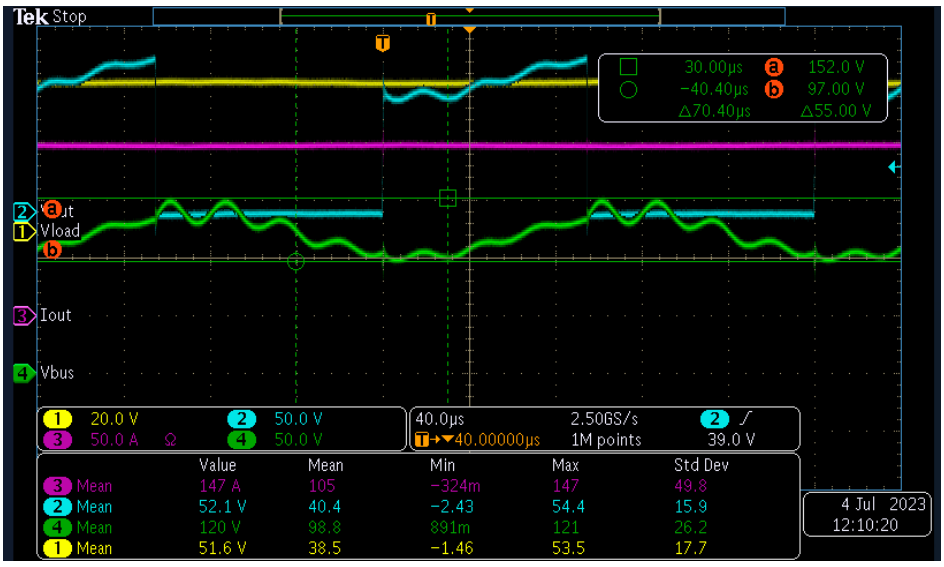

Figure 14. Converter performance under normal operating conditions: V_{LOAD} (yellow), V_{DC} (green), I_{LOAD} (purple), and V_{OUT} (blue).

Table 3. DC-DC converter performance at different operating points.

V_{DC}	Duty Cycle	V_{LOAD}	I_{LOAD}
80 V	0.5	35.7 V	102 A
100 V	0.5	44.6 V	128 A
110 V	0.5	49.2 V	141 A
120 V	0.48	51.6 V	147 A

6.3. Module Controller Synchronization

The purpose of this test is to validate the synchronization via EtherCAT communication between a string controller and two module controllers operating simultaneously, depicted in the set-up diagram of Figure 15.

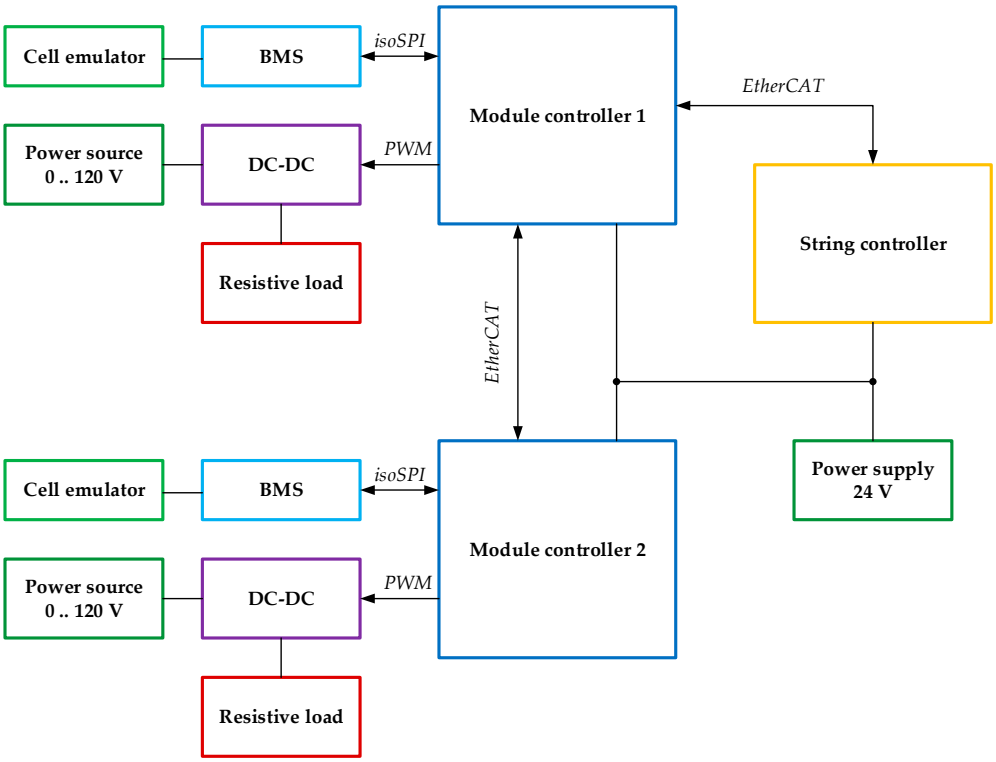

Figure 15. Synchronization test set-up diagram.

To ensure the synchronization of both module controllers with the string controller, a test was conducted where the two associated DC-DC converters switched simultaneously. The string controller sampling period is $T_{S-string}$ = 400 µs, and the switching frequency of the converters is f_{sw} = 5 kHz, which is a period of 200 µs. Figure 16 shows the output voltage waveforms of Module 1 (dark blue) and Module 2 (light blue) in the same string. Both modules operate with the same duty cycle to ease the measurement. The oscilloscope triggers every time Module 1 switches on, and it is configured in "Persistent mode" to capture and overlay several triggered events continuously. Therefore, the variation in deviation between the switching instants for Module 1 and Module 2 can then be observed.

Figure 16 shows that the two modules are switched simultaneously, i.e., their output voltage goes from 0 V to 50–54 V at the same instant, but there is an activation delay between them. However, the accuracy of the synchronization is very high, based on the result obtained in Figure 16, which shows a maximum deviation of around +/−200 ns. This is low enough to avoid any significant additional current ripple due to the non-synchronized switch-on and switch-off of the modules in series.

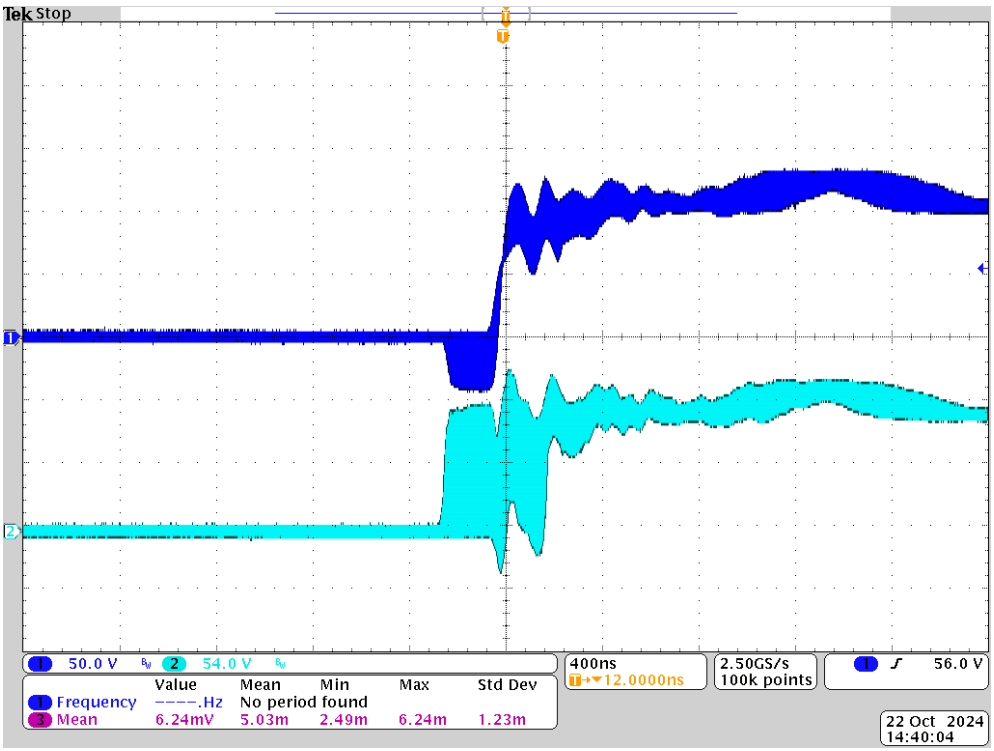

Figure 16. Module 1 (dark blue) and Module 2 (light blue) output voltage waveforms from switch-off to switch-on state with the oscilloscope configured in persistent mode. The maximum deviation observed between both modules' switch-off to switch-on transition is 200 ns.

The tests shown from here onwards are tests of a larger part of the system. The testing environment is a power hardware-in-the-loop (P-HIL) laboratory, in which some of the components are real components, but most of them are emulated by a real-time simulator and controlled voltage sources. The P-HIL set-up consists of two real hardware modules and the associated components. The set-up is used for testing the hardware and software of the master controller, string controller, and module controller, including the DC-DC controller and the BMS system.

Six modules connected in series form each string. The load profile used in the experimental validation has been modified to obtain meaningful results. Due to limited current capacity of laboratory DC sources that emulate batteries, as well as the absence of cooling for the DC-DC converters, the load current amplitude has been scaled-down by a factor of 0.045 (e.g., 200 A in simulation are 9 A in experimental tests). Time is also scaled by a factor of five, from $t = 1$ s in simulation to $t = 5$ s in laboratory tests, such that it is easier to see the results. The DC bus voltage is also scaled down by a factor of four, maintaining the reference at $V^*_{DC} = 250$ V. The LPF time constant implemented for the power split algorithm is of $\tau = 1$ s. These modifications apply for all the tests using the load profile.

6.4. HESS Current Control Mode

In this control mode, the HESS allows setting of the total HESS current reference (I^*_{HESS}) in open loop, while another source connected in parallel maintains the DC bus voltage at its nominal level. Then, the LPF splits I^*_{HESS} in HE and HP current references. The string controllers operate in closed-loop current control with setpoint from the HESS controller. Figure 17 shows the HE string current I_{HE} (red), the HP string current I_{HP} (yellow), and the sum of both strings (blue). I^*_{HESS} starts at 0 A, then it increases to 10 A, and finally decreases to −10 A.

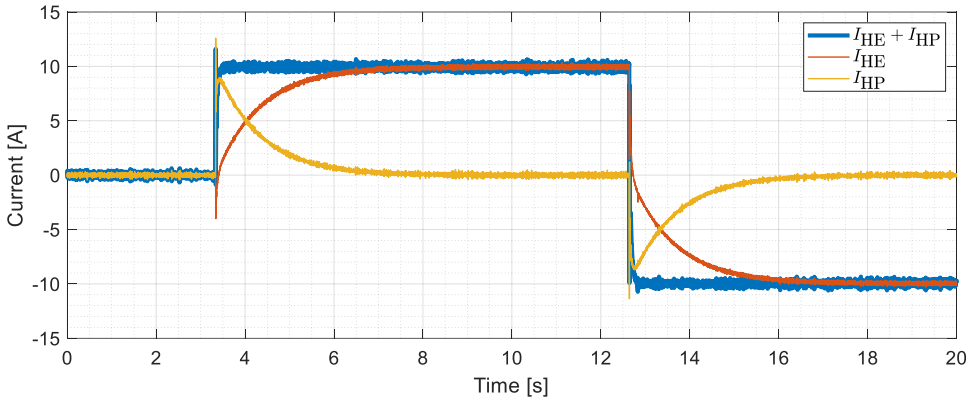

Figure 17. Direct current control mode. HE and HP current and total current measurements.

6.5. Combined Control Mode

This test aims at validating the operation of the HESS combining both, battery power flow, and voltage control modes, with each mode implemented in different strings. The HP string is in charge of maintaining the DC bus voltage level at $V_{DC} = 250$ V, while the HE string is in charge of delivering $P_{HE} = 1$ kW of power to the DC bus. Figure 18a shows HP current (I_{HP}), HE current (I_{HE}), and the total current delivered to the load ($I_{HE} + I_{HP}$), together with the load current demand (I_{LOAD}). Power flows corresponding to the currents in Figure 18a are shown in Figure 18b, where the HE string regulates the delivered power at $P_{HE} = 1$ kW, and the HP string compensates the power difference (P_{HP}) between P_{HE} and the load power (P_{LOAD}). Finally, Figure 18c shows V_{DC} waveform fluctuation corresponding to the power flow in this control mode.

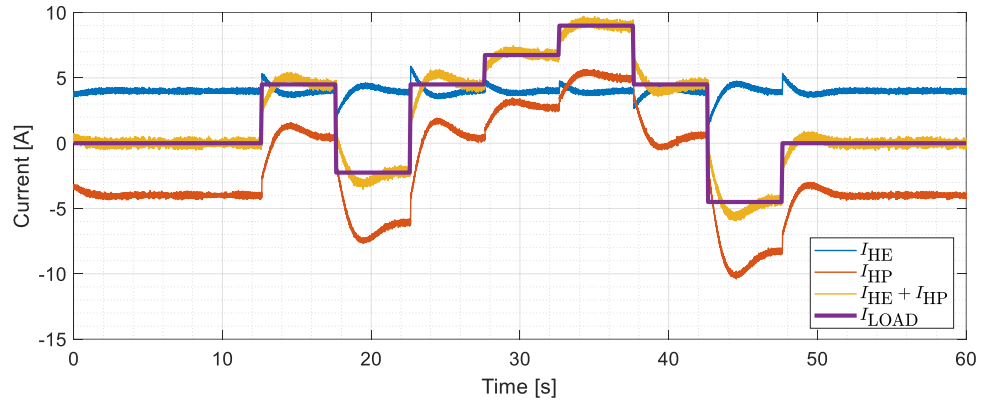

(**a**)

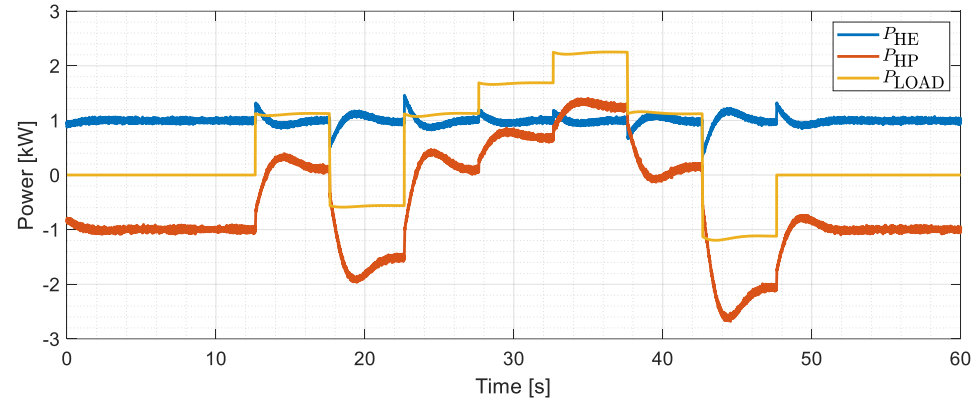

(**b**)

Figure 18. *Cont.*

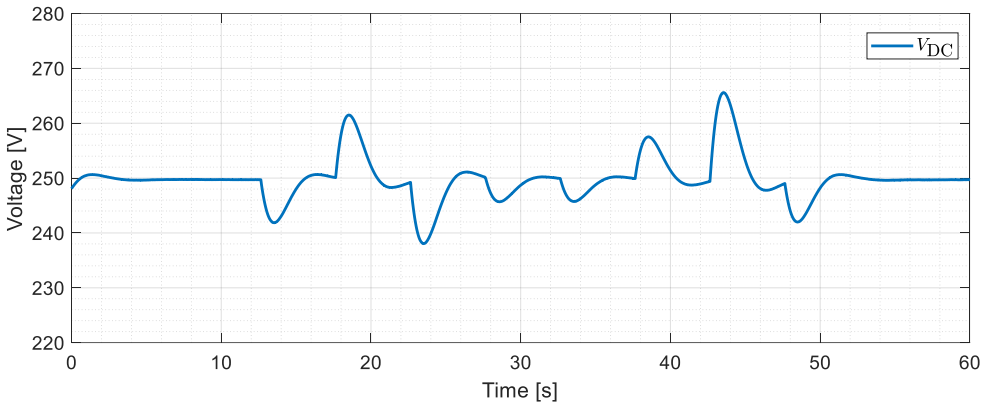

(**c**)

Figure 18. Experimental results of the HESS adopting the combined control mode. (**a**) HE and HP string currents, total current, and load current profile. (**b**) HE and HP string powers and load powers. (**c**) DC bus voltage.

6.6. Droop Control Mode at the String Level

The objective of this test is to validate droop control mode at the string level, with both HE and HP strings responsible for maintaining the DC bus voltage at $V_{DC} = 250$ V. The HE string employs a droop gain of 2 V/A, while the HP string utilizes a droop gain of 4 V/A. These values are intentionally set high to clearly demonstrate the effect of droop control using different droop gains. This approach also minimizes the impact of voltage measurement offsets in the two strings, as the tests were performed at low current and voltage levels. Note that the LPF for current sharing is not active in this case. Instead, the droop gains are responsible for determining the current sharing. Figure 19a illustrates that the HE string provides twice the current of the HP string due to the droop gain settings applied to each of them. Figure 19b shows the voltage variations as a consequence of the load demand in this control mode.

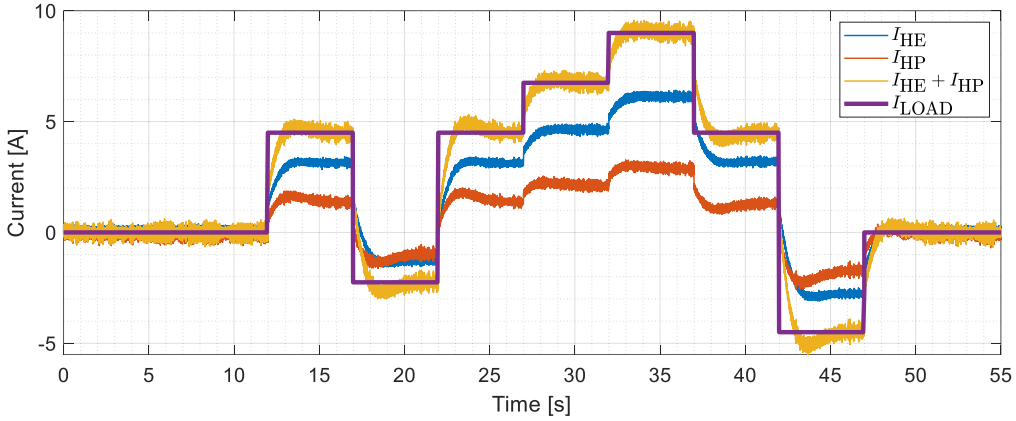

(**a**)

Figure 19. *Cont.*

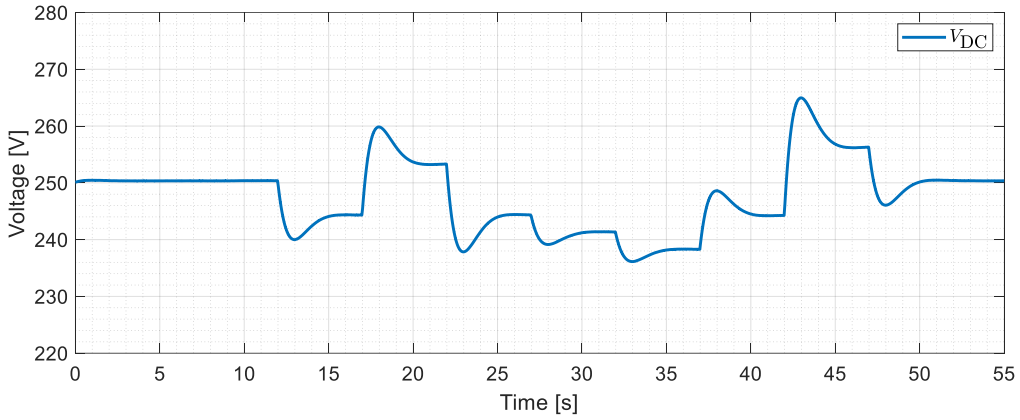

(**b**)

Figure 19. HESS system results adopting droop control mode at the string level. (**a**) HE and HP current and total current measurements and load current profile. (**b**) DC bus voltage.

6.7. HESS Master Voltage Control Mode

Figure 20 shows the HESS response when adopting the closed-loop voltage control operating mode. Figure 20a illustrates the currents of HE and HP strings meeting the load demand, while Figure 20b depicts the DC bus voltage waveform and the perturbations occurring with each change in the load demand.

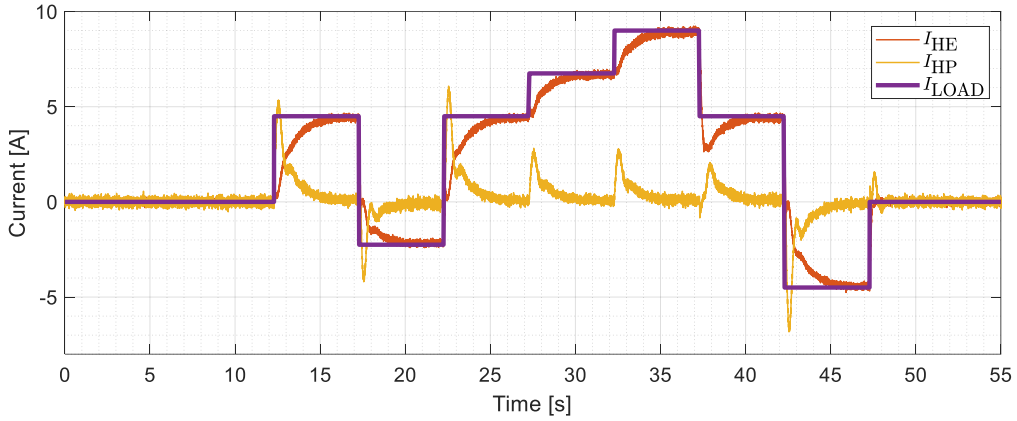

(**a**)

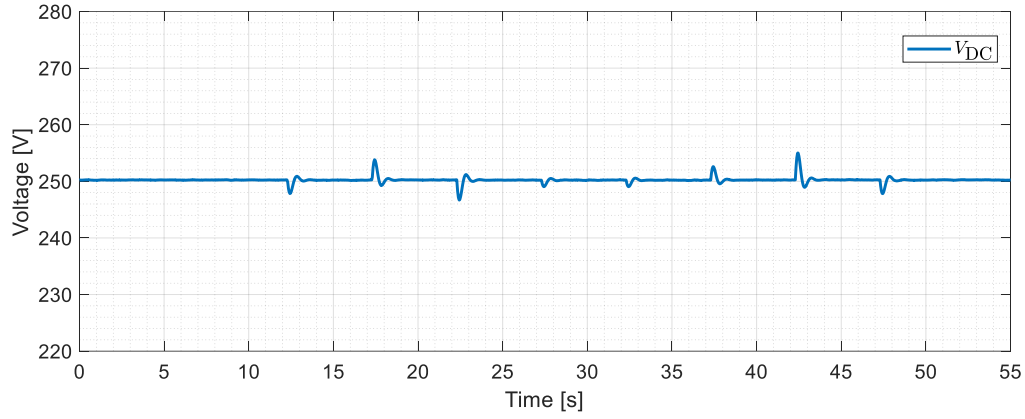

(**b**)

Figure 20. Experimental results adopting HESS master voltage control. (**a**) HE and HP current measurements and load current profile. (**b**) DC bus voltage.

6.8. HESS Master Droop Control Mode

Figure 21 shows the operation of the HESS system and an additional source operating in parallel. Both implement droop control with the same gain of $K_{\text{droop}} = 2\,\text{V/A}$. Figure 21a illustrates the currents of the HE and HP strings and the additional source that meets the load demand, while Figure 21b depicts the V_{DC} waveform where the variation in V_{DC} is influenced by the load demand and the droop gain implemented in each of the sources. It is evident that in the steady state, the additional source and the HE string share the current equally, as expected, due to their identical droop characteristics. Since the HP string contributes only during transients, the HE string and the additional source do not follow each other despite having the same droop. This is because the current sharing algorithm adjusts the current reference for the HE string.

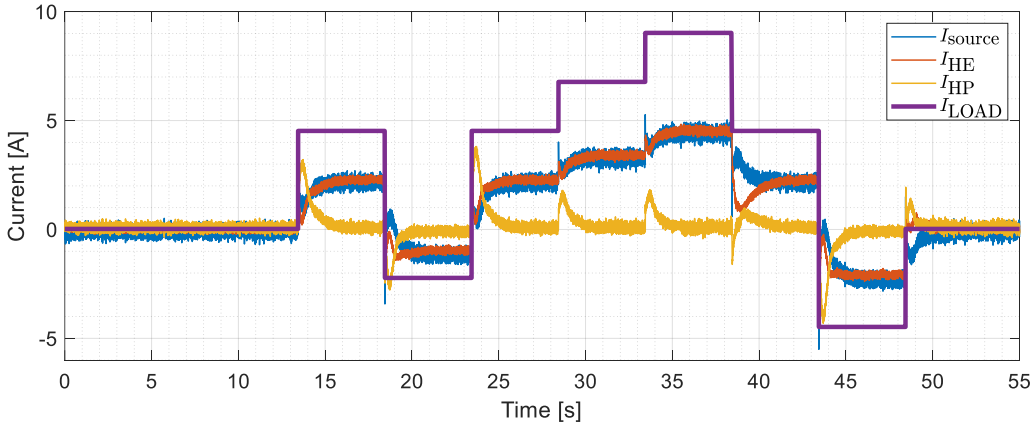

(**a**)

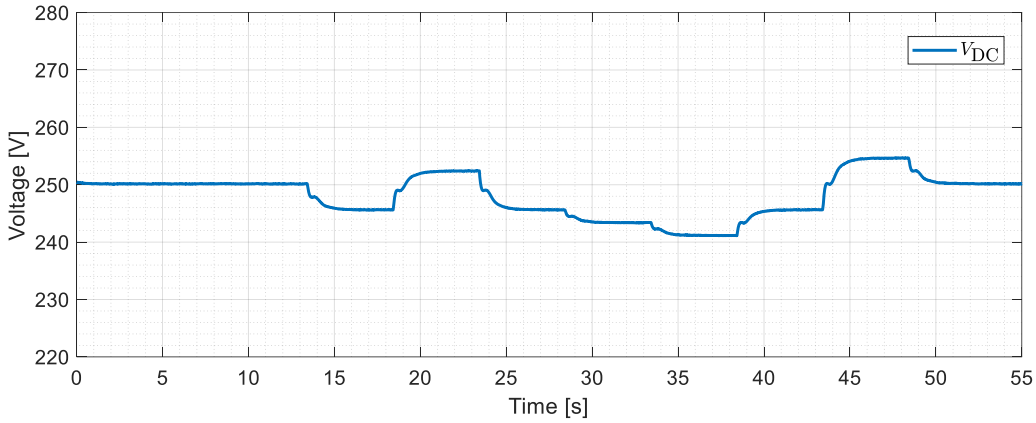

(**b**)

Figure 21. HESS experimental results adopting HESS master droop control. (**a**) Currents of the additional source, the HE and HP strings, and the load. (**b**) DC bus voltage.

6.9. Balancing Open Circuit Voltage of the Modules Within the Same String

One of the advantages of the modular converter design is the ability to balance the voltage of all modules within the same string. In a traditional design, with a common DC-DC converter for the whole system, the current will be the same through all modules within the same string. The utilization of the modules will then be limited by the module with the lowest capacity. Charging and discharging need to stop when the SoC reaches maximum or minimum, respectively. Over time, as degrading increases, the module with the weakest cell will limit the utilization of the full capacity of the other modules within the same string. Even worse, since in a traditional system, the strings are in direct parallel,

any weak module in the system will limit the full utilization of the capacity of the other strings as well.

This disadvantage can be reduced with the modular design. The string controller manages the load sharing between the modules connected to it so that their internal battery voltages are kept at the same level (and, thus, at the same percent of SoC). In this way, the weakest cell will only limit the utilization of the full capacity of its own module. The other modules in the string will not be affected (they will, however, still be limited by their own weakest cell).

Test results related to the voltage balancing functionality are shown in Appendix C, where the real full system of twelve series-connected modules is tested in discharging mode. The results show the convergence of the module voltages made possible by the modular converter approach.

7. Conclusions

In this paper, the combination of HP and HE batteries into a vessel's electrical system has been achieved through the integration of highly efficient modular DC-DC converters.

The hybrid topology that combines HE battery cells and HP battery cells reduces the size of the energy storage system while providing sufficient energy and power to meet the ship's demands. Additionally, this hybrid approach removes the high-current stress factor from the HE battery, resulting in a longer lifetime and smaller temperature peaks in the cells and minimizing the effects of a high depth of discharge.

Moreover, integrating hybrid energy storage technologies with power electronic converters in a modular solution allows for flexible capacity adjustments and makes the systems scalable, ensuring that vessels can adapt to changing operational requirements. A modular system offers independent power flow control for each module, extending the ESS's lifetime and equalizing degradation across modules. Furthermore, the modular design enhances reliability, as defective modules can be bypassed, keeping the battery string operational until replacements are made. This approach also generates cost savings by eliminating the need for strict matching of module characteristics, allowing the use of different generations of batteries within the same string, which is a significant advantage given the rapid development of cell technology.

Finally, the research highlights the practical application of hybrid and modular solutions, integrating various battery cell technologies with simple power electronic converters that require fewer components and less complex control systems.

However, modular systems require robust control structures to ensure correct and reliable operation. Therefore, the incorporation of a hierarchical control guarantees an efficient and safe operation of the HESS system that can be adapted to the different operation modes of the vessel (such as departure, maneuvering, navigation, docking, etc.).

Specifically, a variety of experimental work and system performance evaluations are provided in this paper to support the above-mentioned benefits.

On the one hand, the implementation of communications based on the EtherCAT standard allows precise synchronization between the DC-DC converters and short cycle times at the string control level, essential in the proposed modular system to maintain system stability and efficiency. This real-time capability has been validated in this research, and related results are presented in this article, showing a synchronization accuracy below 200 ns between two modules and a stable control at a cycle time of 400 µs. In addition, in communication links where cycle times are in the order of 10 ms or above, and synchronization is not critical, the use of CAN bus for communication of the HESS master controller with the string controllers and with the HMI ensures robustness and reliability in data transmission.

On the other hand, the system shows the ability to power up without a precharge circuit, as current control allows for connection without any current flow. It is demonstrated that the system can handle different power demand scenarios, maintaining the stability of the DC bus and optimizing the power flow between the HE and HP cells. Moreover, functionalities such as SoC balancing on the batteries of the same string are noteworthy.

Thus, the results obtained in both simulations and experimental tests validate the feasibility of the proposed approach in real-world scenarios.

Author Contributions: Conceptualization, R.L.-E., A.A., and O.M.; software, A.L.-d.-H., G.G., A.L., A.A., and R.L.-E.; validation, A.L.-d.-H., M.A., G.G., and O.M.; formal analysis, R.L.-E., A.L., and A.A.; writing—original draft preparation, R.L.-E., A.L., and A.A.; writing—review and editing, R.L.-E., A.L., O.M., and G.G.; supervision, A.A.; project administration, A.A.; funding acquisition, A.A. All authors have read and agreed to the published version of the manuscript.

Funding: This research received funding from the European Union under grant agreement no. 963560 Horizon 2020 SEABAT—"Solutions for largE bAtteries for waterBorne trAnsporT". It reflects only the authors' views, and the Agency is not responsible for any use that may be made of the information it contains.

Data Availability Statement: The original contributions presented in this study are included in the article. Further inquiries can be directed to the corresponding author(s).

Conflicts of Interest: Authors Giuseppe Guidi and Olve Mo were employed by the company SINTEF Energy AS. Authors Amaia Lopez-de-Heredia and Mikel Alzuri were employed by the company IKERLAN. The remaining authors declare that the research was conducted in the absence of any commercial or financial relationships that could be construed as a potential conflict of interest.

List of Abbreviations

Acronym	Description
BESS	Battery energy storage system
BMS	Battery management system
CoE	CANopen over EtherCAT
ESS	Energy storage system
EV	Electric vehicle
GHG	Greenhouse gas
HE	High energy
HESS	Hybrid energy storage system
HMI	Human–machine interface
HP	High power
IMD	Insulation monitoring device
IMO	International Maritime Organization
LIB	Lithium-ion batteries
LPF	Low-pass filter
LTO	Lithium titanate oxide
M3C	Modular multilevel matrix converter
NMC	Nickel manganese cobalt oxide
P-HIL	Power hardware-in-the-loop
PWM	Pulse-width modulation
SoC	State of charge
SOEM	Simple open EtherCAT master
SoF	State of function
SoH	State of health
VMS	Vessel management system

Appendix A. Test Bench Set-Up Details

This Appendix includes additional information about the different test bench set-ups used to obtain the experimental results in Section 6.

Appendix A.1. DC-DC Converter Characterization

The experimental set-up used for the DC-DC converter characterization in Section 6.1 is detailed in Figure A1, composed of 4 EA PSB 10000 4U power supplies connected in parallel, each supplying 40 A and 160 A in total, to emulate the battery cells. The test platform also includes a Yokogawa WT1806E power analyzer to measure the converter's input and output voltages and currents using passive voltage probes and LEM 205-S Ultrastab current transducers. The data acquisition system used is an Agilent 34970A datalogger. Tests are carried out at ambient temperature.

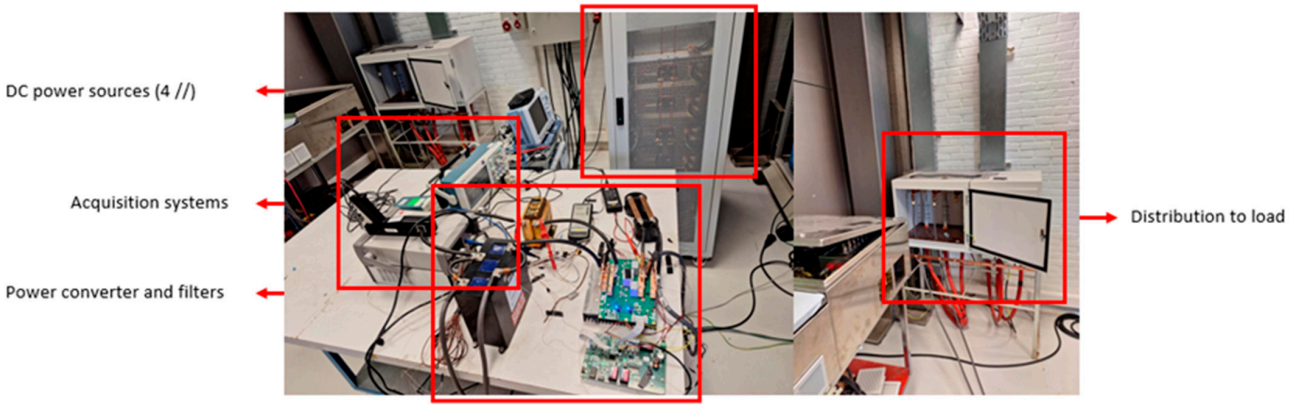

Figure A1. Buck mode operation experimental set-up.

Appendix A.2. Single Module Validation Under Normal Operating Conditions

The experimental set-up used for the single-module validation described in Section 6.2 is detailed in Figure A2. In this set-up, the power supply used to emulate the battery cells has the capacity to deliver 94 A and 160 V. Since the objective is to validate the complete module (DC-DC + BMS), passive loads were used for the DC-DC (a 0.35 Ω resistor and a 3.5 mF capacitor), and cell emulators were employed to validate the BMS. The required voltages and currents were measured using passive probes and an oscilloscope (TEKTRONIX MDO 3054).

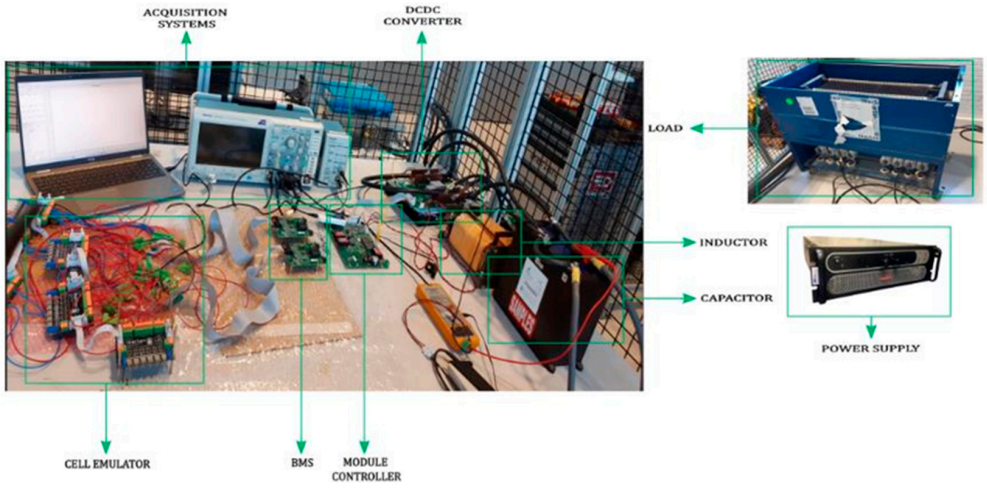

Figure A2. DC-DC converter, BMS and module controller experimental set-up.

Appendix A.3. Module Controller Synchronization

The experimental set-up used for module controller synchronization described in Section 6.3 is detailed in Figure A3. In this test, two DC-DC converters and two module controllers were required to validate synchronization. The objective was to verify synchronization; therefore, no load was added, as the goal was not to supply power. Synchronization between both modules was defined using the string controller. Additionally, cell emulators were employed to enable the use of the BMS. The required voltages and currents were measured using passive probes and an oscilloscope (TEKTRONIX MDO 3054).

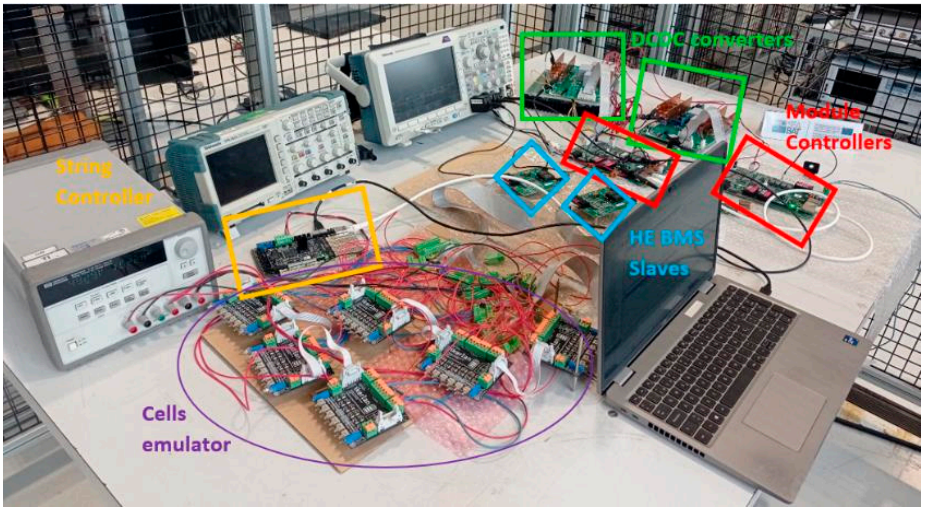

Figure A3. Module's synchronization experimental set-up.

Appendix B. Data Transfer Details in Communications

Section 4 describes communication levels' functionality within the whole system, their topologies, and their relationship with the system control from both functional and real-time requirement perspectives. In this Appendix, on the other hand, details about data transfer in these communication levels are given.

Appendix B.1. String Level

The application layer protocol in this communication level is CoE, which is ultimately CANopen, so all the transmitted and received information is structured in three main types of communication frames or data objects, which are synchronization frames, Process Data Objects (PDOs), and Service Data Objects (SDOs). Figure A4 illustrates the communication flow at the string level.

In this system, the string control cycle has been set at 400 µs, which is achieved by synchronization frames (SYNC0) commonly sent from the string controller to all the module controllers in the link. Module controllers use SYNC0 events to synchronize the internal PWM generator, which means that the resulting switching frequency of each DC-DC converter must be an integer multiple of the string control cycle frequency (2.5 kHz for the defined 400 µs string control cycle).

PDOs include information needed to perform the control of the string, such as operating commands and PWM duty cycle reference from the string controller to the module controllers and operation state and battery voltage measurements from module controllers to the string controller.

SDOs do not exchange necessary data to carry out the control of the string. Sporadically, monitoring information is principally transmitted in SDOs, like module temperature, cell voltage, etc.

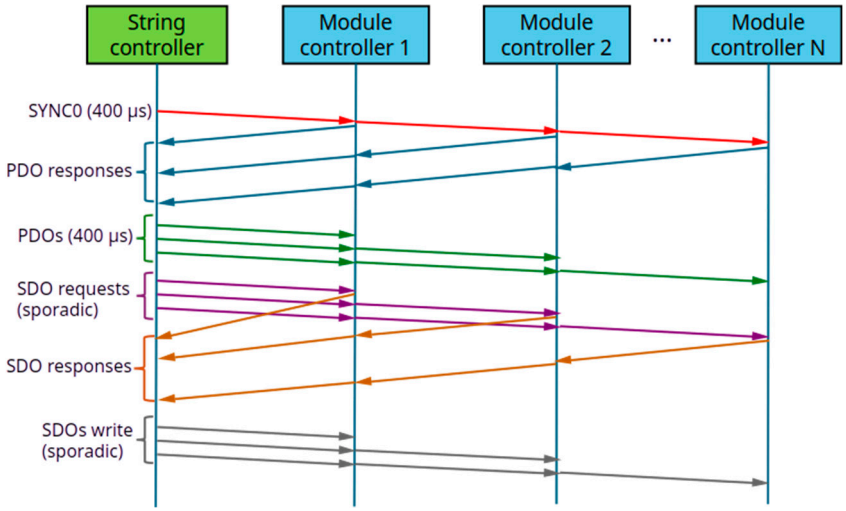

Figure A4. EtherCAT sequence diagram during normal operation of the bus.

Appendix B.2. HESS Level

Also, at this level, the transmitted information is structured in the same three types of communication objects as in the string level: synchronization frames, PDOs, and SDOs. Figure A5 illustrates the communication flow between the HESS master controller and the string controllers.

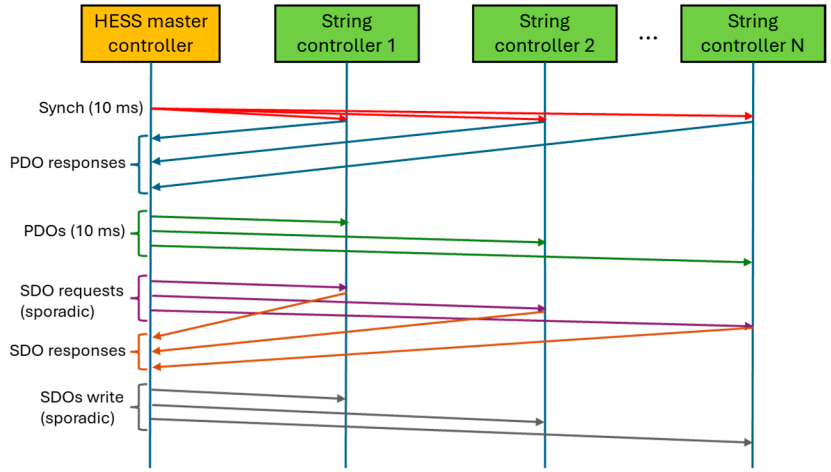

Figure A5. HESS level communication sequence diagram.

As shown in Figure A5, synchronization frames and PDOs are exchanged at a regular interval of 10 ms, which is the cycle time in the HESS control level. The string controllers send their PDOs in response to the synchronization frames of the HESS master controller, while the PDOs sent by the HESS master controller are generated independently at the same regular interval.

PDOs include information needed to perform the control of the system, such as operating commands and voltage or current references from the HESS master controller to string controllers and operation state and voltage or current measurements from string controllers to the HESS master controller.

SDOs are sporadically exchanged on the HESS master controller's demand. Contrary to the PDOs, SDOs do not exchange necessary data to carry out the control of the system, which is why time intervals between SDOs can be longer than the control cycle, and network overload can be avoided. Monitoring information is principally transmitted in SDOs, like string SoC, module voltage, cell temperature, etc.

Appendix B.3. HMI Level

Figure A6 illustrates the communication flow at this level. The HESS master controller sends 70 monitoring CAN messages, which include various system information, to the HMI cyclically every 100 ms. In contrast, it receives commands from the HMI sporadically, on user demand, with each command consisting of a single CAN message. Additionally, to ensure that the HMI is active, it sends a Keep Alive (KA) frame to the HESS master controller every 100 ms. Regarding the IMD, this device only communicates with the HESS master controller and is transparent to the HMI. The HESS master controller polls for insulation status information every 100 ms, to which the IMD responds with the requested data.

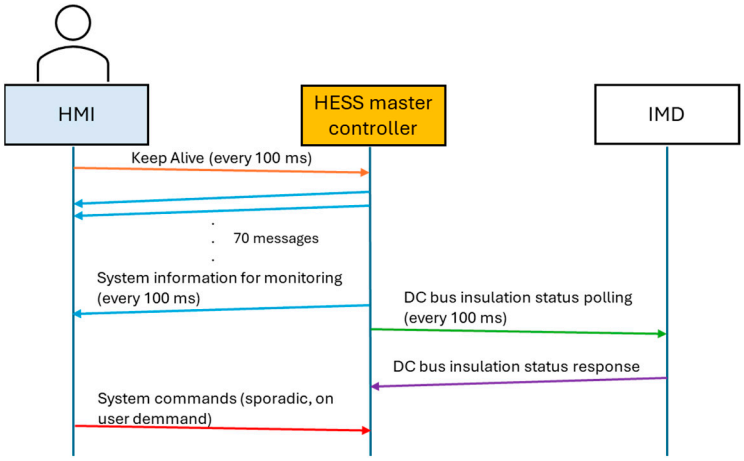

Figure A6. Communication flow between the HESS master, HMI, and IMD.

Appendix C. Additional Experimental Results: Module SoC Balancing

This Appendix provides additional information about the HESS system performance. Specifically, it includes experimental results related to module voltage balancing within the same string and the duty cycle of the modules in a string. These measurements are taken from a test of the full system with 12 real modules in the string (not hardware in the loop). Figure A7 shows a constant-current discharge process of several modules in a string, with string current regulated to 40 A. The logging includes five of the modules, but twelve modules were included in the test. Before starting the discharge test, the modules were deliberately charged to different voltages (or SoC) to highlight the balancing effect. Among the modules shown, Module 1 and Module 3 have the highest initial SoC, Module 7 and Module 11 have the lowest, and Module 4 is at an intermediate voltage level. While the result does not cover the full-time interval towards full convergence, the trend towards voltage balance between modules of the same string is clearly visible. In the logging, some of the measured module voltages (7, 11, and 12 after 250 s) look considerably noisier. This is due to the fact that such modules are operated in PWM mode during the balancing process. The range of variation of the measured voltage related to those modules corresponds to the voltage drop due to the passage of the string current.

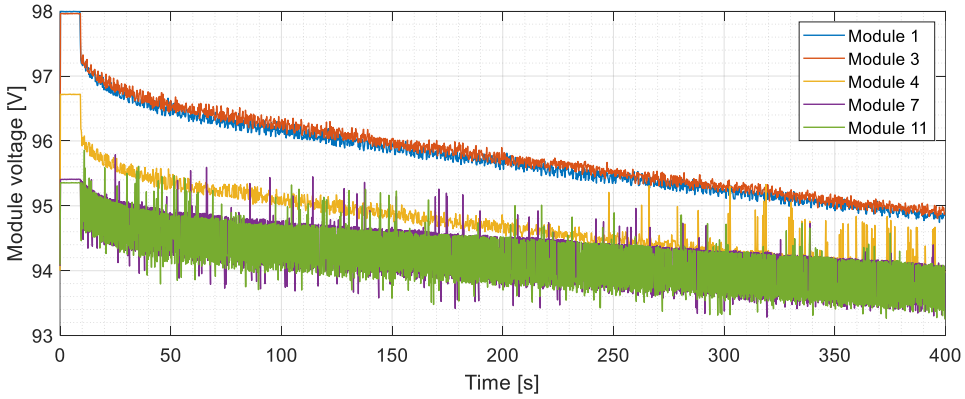

Figure A7. SoC balancing between modules of the same string.

Appendix D. Additional Experimental Results: Duty Cycle Details

Figure A8a illustrates the duty cycle of all six modules in the HP string with a detailed view provided in Figure A8b. This operation corresponds to the experimental result in Section 6.7. These figures demonstrate that the string controller alternates the active module. Notably, five of the modules exhibit duty cycle values of either 0 or 1, while the sixth module displays a duty cycle value ranging between 0 and 1.

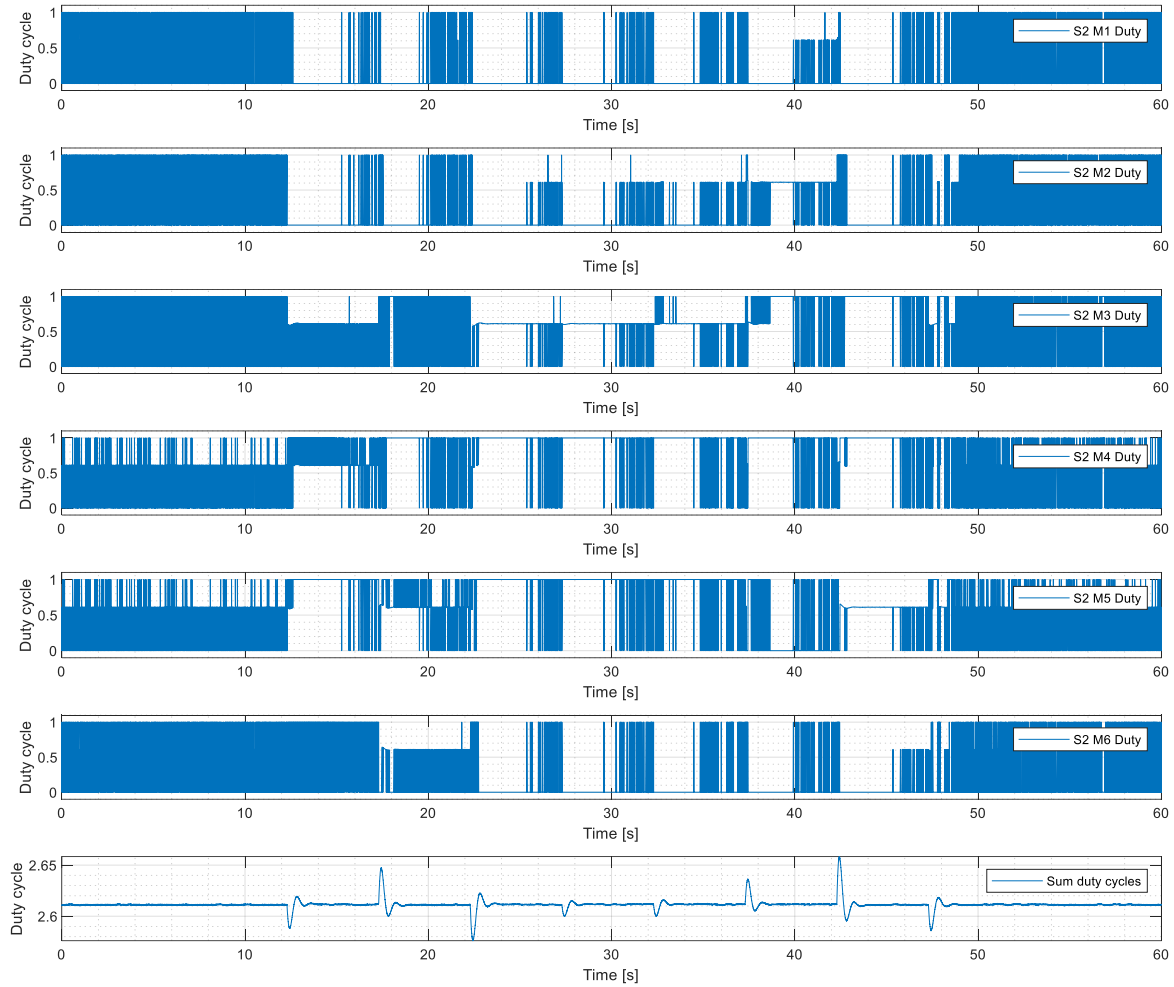

(**a**)

Figure A8. *Cont.*

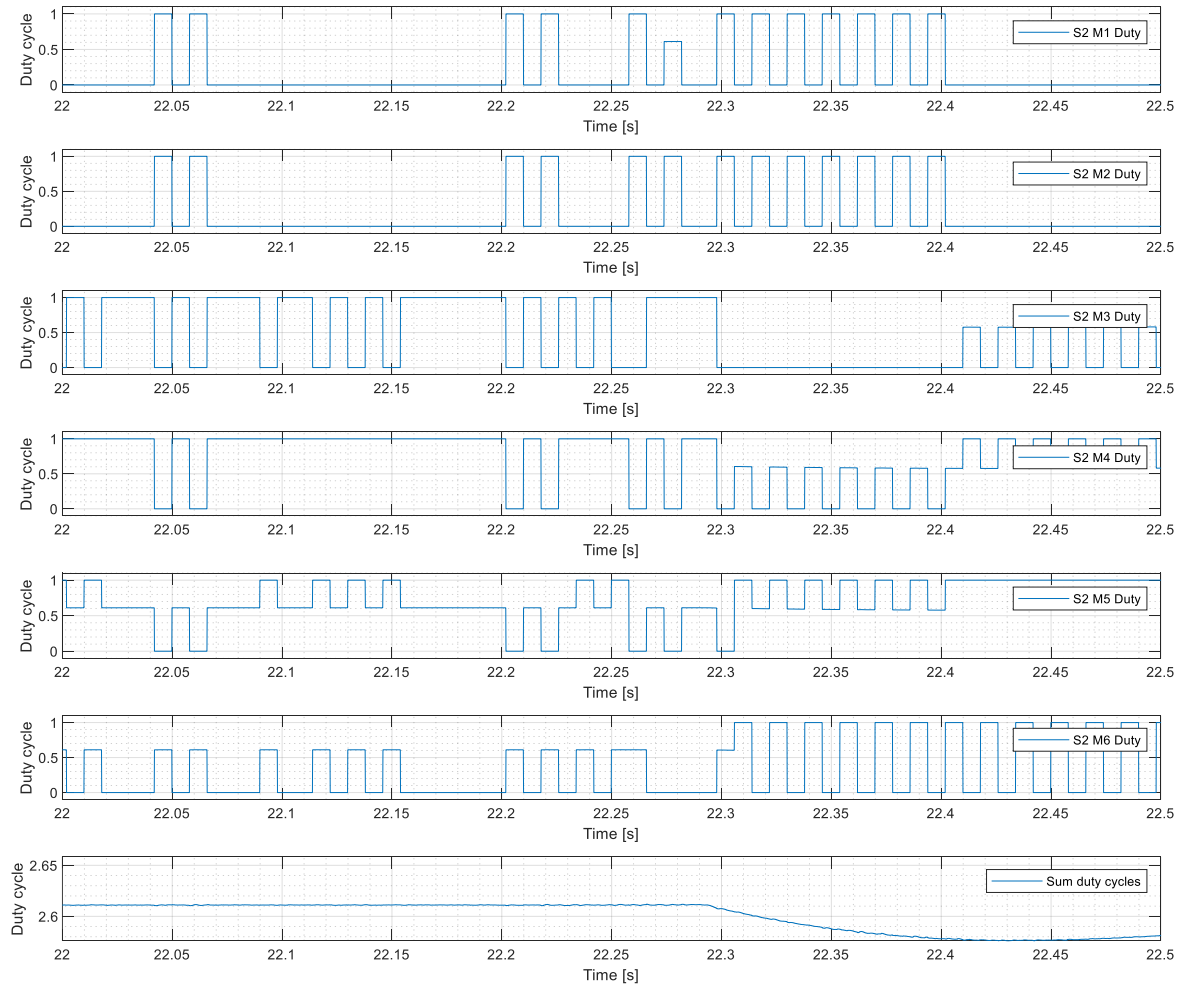

(**b**)

Figure A8. (**a**) Duty cycle operation of the six modules in the HP string and (**b**) a zoomed view corresponding to the experimental results in Section 6.7: HESS master voltage control mode.

References

1. European Environment Agency. *Rail and Waterborne-Best for Low-Carbon Motorised Transport Rail and Waterborne*; European Environment Agency: Copenhagen, Denmark, 2023.
2. International Maritime Organization (IMO). *2023 IMO Strategy on Reduction of GHG Emissions from Ships*; International Maritime Organization (IMO): London, UK, 2023.
3. United Nations Conference on Trade and Development (UNCTAD). Review of Maritime Transport 2023-Towards a Green and Just Transition. 2023. Available online: https://shop.un.org/ (accessed on 27 December 2024).
4. Choi, E.; Kim, H. Advanced Energy Management System for Generator–Battery Hybrid Power System in Ships: A Novel Approach with Optimal Control Algorithms. *J. Mar. Sci. Eng.* **2024**, *12*, 1755. [CrossRef]
5. Gagatsi, E.; Estrup, T.; Halatsis, A. Exploring the Potentials of Electrical Waterborne Transport in Europe: The E-ferry Concept. In *Transportation Research Procedia*; Elsevier B.V.: Amsterdam, The Netherlands, 2016; pp. 1571–1580. [CrossRef]
6. Wu, P.; Bucknall, R. Marine propulsion using battery power. In Proceedings of the Shipping in Changing Climates Conference, Newcastle, UK, 10–11 November 2016.
7. Mandrile, F.; Martino, M.; Musumeci, S.; Pastorelli, M. Hybrid battery systems: An investigation for maritime transport. *Int. J. Energy Prod. Manag.* **2023**, *8*, 141–147. [CrossRef]
8. Barone, G.; Buonomano, A.; Del Papa, G.; Maka, R.; Palombo, A. Approaching zero emissions in ports: Implementation of batteries and supercapacitors with smart energy management in hybrid ships. *Energy Convers. Manag.* **2024**, *314*, 118446. [CrossRef]
9. Kolodziejski, M.; Michalska-Pozoga, I. Battery Energy Storage Systems in Ships' Hybrid/Electric Propulsion Systems. *Energies* **2023**, *16*, 1122. [CrossRef]

10. Bei, Z.; Wang, J.; Li, Y.; Wang, H.; Li, M.; Qian, F.; Xu, W. Challenges and Solutions of Ship Power System Electrification. *Energies* **2024**, *17*, 3311. [CrossRef]
11. Trombetta, G.L.; Leonardi, S.G.; Aloisio, D.; Andaloro, L.; Sergi, F. Lithium-Ion Batteries on Board: A Review on Their Integration for Enabling the Energy Transition in Shipping Industry. *Energies* **2024**, *17*, 1019. [CrossRef]
12. Mathieu, R.; Briat, O.; Gyan, P.; Vinassa, J.M. Comparison of the impact of fast charging on the cycle life of three lithium-ion cells under several parameters of charge protocol and temperatures. *Appl. Energy* **2021**, *283*, 116344. [CrossRef]
13. Jagfeld, S.M.P.; Birke, K.P.; Fill, A.; Keil, P. How Cell Design Affects the Aging Behavior: Comparing Electrode-Individual Aging Processes of High-Energy and High-Power Lithium-Ion Batteries Using High Precision Coulometry. *Batteries* **2023**, *9*, 232. [CrossRef]
14. Elsayed, A.T.; Mohammed, O.A. A Comparative Study on the Optimal Combination of Hybrid Energy Storage System for Ship Power Systems. In Proceedings of the 2015 IEEE Electric Ship Technologies Symposium (ESTS), Old Town Alexandria, VA, USA, 21–24 June 2015.
15. Camara, M.B.; Payman, A.; Dakyo, B. Energy management based on frequency approach in an electrical hybrid boat. In Proceedings of the 2016 International Conference on Electrical Systems for Aircraft, Railway, Ship Propulsion and Road Vehicles & International Transportation Electrification Conference (ESARS-ITEC), Toulouse, France, 2–4 November 2016. [CrossRef]
16. Hossain Lipu, M.S.; Miah, M.S.; Ansari, S.; Meraj, S.T.; Hasan, K.; Elavarasan, R.M.; Mamun, A.A.; Zainuri, M.A.A.M.; Hussain, A. Power Electronics Converter Technology Integrated Energy Storage Management in Electric Vehicles: Emerging Trends, Analytical Assessment and Future Research Opportunities. *Electronics* **2022**, *11*, 562. [CrossRef]
17. Gajardo, J.; Pereda, J.; Mora, A. Modular Multilevel Matrix Converter with Hybrid Energy Storage for Propulsion Systems and Grid Supply in Marine Vessels. In Proceedings of the 2023 IEEE 8th Southern Power Electronics Conference and 17th Brazilian Power Electronics Conference (SPEC/COBEP), Florianopolis, Brazil, 26–29 November 2023; IEEE: Piscataway, NJ, USA, 2023; pp. 1–7. [CrossRef]
18. Long, W.; Liu, N.; Wang, K.; Xu, X.; Zheng, Z.; Li, Y. A Modular Multilevel Converter with Integrated Composite Energy Storage for Ship MVDC Electric Propulsion System. In Proceedings of the 2020 IEEE 9th International Power Electronics and Motion Control Conference, IPEMC 2020 ECCE Asia, Nanjing, China, 29 November–2 December 2020; IEEE: Piscataway, NJ, USA, 2020; pp. 824–829. [CrossRef]
19. Anzola, J.; Garayalde, E.; Urkizu, J.; Alacano, A.; Lopez-Erauskin, R. High Efficiency Converters Based on Modular Partial Power Processing for Fully Electric Maritime Applications. *Electronics* **2023**, *12*, 2778. [CrossRef]
20. Fu, Y.; Lu, Z.; Yan, X. Integrated power system for battery-only electric ship. 2018.
21. Ayers, W.N. Batteries and DC Shore Charging for High-Speed Electric Vessels. In Proceedings of the SNAME Maritime Convention, SNAME, Norfolk, VI, USA, 14–16 October 2024. [CrossRef]
22. He, W.; Valøen, L.O.; Olsen, K.V.; Kjeka, K.M.; Fredriksen, B.M.; Petiteau, M.; Touat, A.; Såtendal, H.; Howie, A.; Howey, D.; et al. Lessons learned from the commercial exploitation of marine battery energy storage systems. *J. Energy Storage* **2024**, *87*, 111440. [CrossRef]
23. Chen, Z.; Wang, B. Design of ship power system with exchangeable battery energy storage containers. In Proceedings of the Ninth International Symposium on Sensors, Mechatronics, and Automation System (ISSMAS 2023), Nanjing, China, 11–13 August 2023; Pan, L., Zhou, Z., Eds.; SPIE: Cergy-Pontoise, France, 2024; p. 133. [CrossRef]
24. Danielis, P.; Skodzik, J.; Altmann, V.; Schweissguth, E.B.; Golatowski, F.; Timmermann, D. Survey on real-time communication via ethernet in industrial automation environments. In Proceedings of the 2014 IEEE Emerging Technology and Factory Automation (ETFA), Barcelona, Spain, 16–19 September 2014; IEEE: Piscataway, NJ, USA, 2014; pp. 1–8. [CrossRef]
25. Wu, X.; Xie, L. Performance evaluation of industrial Ethernet protocols for networked control application. *Control Eng. Pract.* **2019**, *84*, 208–217. [CrossRef]
26. Sridevi, G.; Saligram, A.; Nattarasu, V. *Effective Protocols for Industrial Communication*; Springer: Singapore, 2019; pp. 1093–1105. [CrossRef]
27. Akbarzadeh, M.; De Smet, J.; Stuyts, J. Battery Hybrid Energy Storage Systems for Full-Electric Marine Applications. *Processes* **2022**, *10*, 2418. [CrossRef]
28. Kistner, L.; Bensmann, A.; Hanke-Rauschenbach, R. Potentials and limitations of battery-electric container ship propulsion systems. *Energy Convers. Manag. X* **2024**, *21*, 100507. [CrossRef]
29. Song, Q.; Loo, K.-H.; Chen, G.; Chen, X.; Mou, D.; Liu, J. An Improved Droop Control Scheme for Enhancing Dynamic Current Sharing Performance in Autonomous DC Microgrids. In Proceedings of the 2024 IEEE 10th International Power Electronics and Motion Control Conference (IPEMC2024-ECCE Asia), Chengdu, China, 17–20 May 2024; IEEE: Piscataway, NJ, USA, 2024; pp. 3369–3373. [CrossRef]
30. Yang, Z.; Min, H.; Yang, F.; Hu, W.; Shen, Y. Hierarchical Control of an Adaptive Droop Regulated Microgrid with Dynamical Load Power Sharing. In Proceedings of the 2024 6th International Conference on Energy Systems and Electrical Power (ICESEP); IEEE: Piscataway, NJ, USA, 2024; pp. 942–947. [CrossRef]

31. EtherCAT. EtherCAT Technology Overview. Available online: https://www.ethercat.org/en/technology.html (accessed on 14 October 2024).
32. EtherCAT. EtherCAT Slave Stack Code (SSC) ET9300. Available online: https://www.ethercat.org/en/products/54FA3235E29643BC805BDD807DF199DE.htm (accessed on 14 October 2024).
33. CANopenNode Project. Available online: https://canopennode.github.io/CANopenNode/ (accessed on 14 October 2024).

Disclaimer/Publisher's Note: The statements, opinions and data contained in all publications are solely those of the individual author(s) and contributor(s) and not of MDPI and/or the editor(s). MDPI and/or the editor(s) disclaim responsibility for any injury to people or property resulting from any ideas, methods, instructions or products referred to in the content.